Impact of Over-exploitation in Coastal Groundwater on the Variations in Submarine Groundwater Discharge Rate in a Complex Two Aquifer System by Finite Element Modelling: A Case Study From South India

Sundara Pandian Rajaveni
Mepco Schlenk Engineering College
Sumadevi Nair Indu
Anna University Chennai
Karthikeyan Brindha
Freie Universität Berlin: Freie Universitat Berlin
Lakshmanan Elango (elango34@hotmail.com)
Anna University https://orcid.org/0000-0002-6692-5773

Research Article

Keywords: coastal aquifer, finite element model, FEFLOW, seawater intrusion, check dams, managed aquifer recharge, Chennai

Posted Date: March 16th, 2021

DOI: https://doi.org/10.21203/rs.3.rs-259927/v1

Version of Record: A version of this preprint was published at Environmental Science and Pollution Research on July 12th, 2021. See the published version at https://doi.org/10.1007/s11356-021-15219-0.

Impact of over-exploitation in coastal groundwater on the variations in submarine groundwater discharge rate in a complex two aquifer system by finite element modelling: A case study from south India

Sundara Pandian Rajaveni [1], Sumadevi Nair Indu [2], Karthikeyan Brindha [3] and Lakshmanan Elango[2 *]

[1] Department of Civil Engineering, Mepco Schlenk Engineering College, Sivakasi -626005, Tamil Nadu, India

[2] Department of Geology, Anna University, Chennai – 600025, Tamil Nadu, India

[3] Hydrogeology Group, Institute of Geological Science, Freie Universität Berlin, 12249 Berlin, Germany

* Corresponding author email: elango@annauniv.edu

Abstract

The purpose of this study is to understand the impact of coastal groundwater over-exploitation on the variations in submarine groundwater discharge (SGD) flux rate and seawater exchange flux across the seabed. As a case study, numerical modelling techniques were applied to a complex multi-aquifer system located north of Chennai, India, which has been affected since the mid-1970s by overexploitation and seawater intrusion. Because of the relatively high hydraulic conductivity, the model shows a higher amount of seawater inflow in the central part of the region. From 2000 to 2012, the movement of seawater has increased from 17,000 m^3/day to 24,500 m^3/day due to groundwater overexploitation from the semi-confined aquifer. However, the quantum of flux from the sea to the aquifer has been reduced from the year 2006 due to the termination of pumping from a well field supplying a part of the city's water supply. Model simulations show that fresh groundwater of 43,312 m^3/day and saltwater of 43,815 m^3/day will be discharged to the aquifer by the end of 2030. In addition to the prevailing condition, various management scenarios were also predicted to prevent the degradation of groundwater quality due to seawater intrusion. By adopting managed aquifer recharge methods, saltwater intrusion (rate of 4408 m^3/day) can be reduced and SGD (rate of 22414 m^3/day) rate

increased. Findings from this study are expected to enhance the understanding of SGD and freshwater budget in coastal areas and in creating integrated coastal management plans.

Keywords: coastal aquifer; finite element model; FEFLOW; seawater intrusion; check dams; managed aquifer recharge; Chennai

Introduction

Submarine groundwater discharge (SGD) is the mechanism by which all fluids (i.e. fresh groundwater, seawater, or a combination of fresh groundwater and seawater) flow from the seabed to the sea through subsurface geological formation. It includes ocean processes such as convection, tidal pumping, and wave set-up. SGD can release terrestrial nutrients, heavy metals, dissolved solids and other potentially harmful contaminants to the coastal environment (Finkl and Krupa 2003, Taniguchi et al. 2002). This process provides a pathway for terrestrial pollutants that can considerably affect the coastal ecosystems where groundwater discharges. The concentration of pollutants in the nearshore water and their effect on the chemistry and biology of the region depends not only on the fluxes of pollutants, but also on the strength of the mixing process and the exchange with the open ocean. The amount of SGD varies spatially and temporally because of variations in recharge, tides, density, hydraulic gradient, complexity and heterogeneity of aquifer formation (Bokuniewicz et al. 2003). Globally, 90 percent of the SGD is estimated to be recirculated by seawater and the remaining 10 percent is SGD freshwater (Kwon et al. 2014). Thus, in order to assess whether SGD is of specific significance, coastal zone managers need to estimate the extent of SGD and the degree of mixing and interaction between the nearshore sea and the open ocean.

Research on SGD has received increased attention since the 1990's as the significance of SGD on coastal zone management was understood and many different investigation methods for quantifying SGD were developed (Moosdorf and Oehler 2017, Taniguchi et al. 2019). Several studies have been carried out to quantify the rate of SGD on the coastal environment based on direct measurements (seepage meter, piezometer, calculation of water budget and Darcy Law) and indirect measurements such as geophysical tracers (conductivity signature, salinity, temperature profiling), separation of hydrographs, natural tracer techniques (radium and radon), geochemical tracers (methane, dissolved silicon, ^{228}Th, silica), natural radioactive isotopes (^{3}H, ^{4}He), stable isotopes (^{2}H, ^{18}O, ^{87}Sr/ ^{88}Sr), thermal imaging, GIS topology, theoretical calculations and numerical models.

Numerical modelling is an important tool used to quantify the amount of fresh groundwater discharge to sea and is being increasingly used recently (George et al. 2018, Welch et al. 2019, Vollberg et al. 2019). These models include the aquifer's nearshore terrestrial portion as well as the marine part below the seafloor, where the effects of density are significant. Detailed understanding of geometry and composition of the aquifer is necessary for successful characterization of an aquifer for SGD modelling (Virtasalo 2019). Fresh submarine groundwater was simulated by using variable-density flow and transport models for understanding complex groundwater flow processes in coastal environments (Langevin 2003) In coastal groundwater systems, Luijendijk et al. (2020) simulated submarine and terrestrial groundwater discharge using a numerical model of combined density-driven groundwater flow and solvent transport that solved the equations of fluid flow and solute transport and the equations of state for fluid density and viscosity in a two-dimensional subsurface cross-section.

India has a long coastline of 7,500 km, and interaction between the freshwater and saline water in these coastal zones are continuous. Several studies have been undertaken in India to learn about the extent of the seawater intrusion and have analyzed the water quality problems in specific locations. Compared to a long coastline of 7,500 km, the number of studies on SGD carried out is less. A summary of the SGD studies carried out in India is given in Table 1. In the present situation, where water shortage is reported in several Indian cities (Pathak 2019), quantification of SGD is important as the groundwater loss in large amounts through the extensive coastline can be used to meet the water requirements for drinking and irrigation (Jacob et al. 2009). With this limited three-dimensional modelling studies on SGD, the understanding of the processes and flux of groundwater from the coastal aquifer to the sea through seabed is also limited. Here, a complex multiple coastal aquifer is used as a case study to simulate the temporal exchange rate of SGD from the coastal freshwater aquifer to sea through the seabed.

Methodology

Description of the study area

The study was carried out in a seawater intruded coastal aquifer which is in the Arani-Korttalaiyar (A-K) river basin, Tamil Nadu, India (Fig. 1), north of the Chennai City. The Arani river originates at Sadasivakonda in Chittoor district, Andhra Pradesh and it joins the Bay of Bengal in Tamil Nadu. The Korttalaiyar river originates near Pallipattu in Thiruvallur district, Tamil Nadu, and flowing in the southern part of the study area, it supplies water to Chozhavaram reservoir and Red Hills lake, thereafter, flows into the Bay of Bengal. Seawater enters these rivers at a distance of about 5 km from the coast when the river does not carry freshwater which was observed during the field survey. The southwestern side of the study area is bounded by the Palar river. This region experiences a very dry period during April to June

100 (summer) with a maximum temperature ranging from 32° C to 44°C and a colder period from
101 December to January (winter) when the temperature ranges from 23°C to 30°C. Precipitation in
102 this region depends on southwest (July to September) and northeast (October to December)
103 monsoons. The average annual rainfall is around 1200 mm, 35% of which occurs during the
104 southwest monsoon (July - September) and 60% during the northeast monsoon (October –
105 December). The topography of this area ranges from sea level (0 m) to 133 m above mean sea
106 level. This area is dominated by dentritic to sub-dentritic drainage pattern mainly dependent on
107 the geological formation. Six wellfields are located in the buried paleo-channel of Palar river
108 (Fig. 1). The tube wells from these wellfields supply water to Chennai, the capital city of Tamil
109 Nadu, located 45 km south of the study area. Agriculture is largely practised and the principal
110 crops grown in this area are rice, sugarcane, banana, vegetables, watermelon, tapioca, pearl
111 millet, cluster bean and pulses such as groundnut, sesame and maize.
112
113 *"Insert Figure 1"*
114
115 **Data collection and field investigation**
116 Survey of India (SOI) toposheets (Scale 1: 25,000) covering the study area were used to prepare
117 the base map. Borehole logs of the study area were collected from the Chennai Metropolitan
118 Water Supply and Sewerage Board (CMWSSB) to characterize the aquifer system.
119 Groundwater head and groundwater abstraction rate from the pumping wells in the wellfield
120 was collected from CMWSSB for the period from January 1990 to December 2012. These
121 pumping wells penetrate more than 30 m depth below ground level which is located in a semi-
122 confined aquifer (shown in Fig. 1). Additionally, the groundwater head from 27 monitoring
123 wells was obtained from the Tamil Nadu Public Works Department (TNPWD) for the
124 calibration of the model (from January 1990 to December 2012). The monthly rainfall from 9

125 rain gauge stations was also obtained from the TNPWD for the time period from January 1990
126 to December 2012.
127
128 A well inventory survey was carried out for 60 wells during January 2011 to locate additional
129 groundwater level monitoring wells for the collection of primary data. Based on this survey,
130 27 dug wells and 22 tube wells were selected as representative wells for regular monitoring of
131 groundwater heads. Groundwater head was measured once in two months from January 2011
132 to December 2013 by using a water level indicator (Solinist 101). In addition to regular
133 monitoring of groundwater head, an intensive field investigation was carried out to measure
134 the groundwater head in several dug and tube wells located very close to each other for
135 characterizing the aquifer system. They dug wells in this area are generally less than 20 m deep
136 and tube wells are up to 120 m deep. About 20 pairs of dug and tube wells located next to each
137 other were chosen to measure groundwater head. In order to convert the groundwater head
138 measured below ground level with respect to the sea level, the elevation of the ground surface
139 was measured using a Differential Global Positioning System (DGPS) (Leica GS09 GNSS).
140
141 ***Geological investigations***
142 Geologically, this area comprises rocks from Archaean to Quaternary age. Crystalline rocks of
143 Archaean age comprising of gneiss and charnockite form the basement. The Upper Gondwana
144 series of shale and clay deposits lie over these crystalline rocks. Tertiary and Quaternary
145 formation lies over the Upper Gondwana formation of a massive pile of lacustrine and fluvial
146 deposits (Rao et al. 2004b). The tertiary formation consists of shale, clay, sandstone and marine
147 sediments. The quaternary formation comprises of laterite and alluvium deposits. Alluvial
148 deposits consist of sand, silt, sandy clay, gravel and pebbles which mostly occur along with the

Arani and Korttalaiyar river courses (Fig. 2a). Sand is the dominant fraction in the alluvial and aeolian deposits which occurs near the coast.

The geological map of the area obtained from the Geological Survey of India (GSI) in 1:50,000 scale was updated by interpreting the IRS 1D LISS-III imagery (2006) of 23.5 m spatial resolution. During the field visit the identified outcrops were cross-checked with the geology map prepared from LISS-III imagery, then it was validated through outcrops. The northwestern and southeastern part of the area is covered by laterite, sandstone and conglomerate. Lineaments play an important role in the groundwater flow. Most of the lineaments are aligned along the west-east direction in the western and central parts of the study area (UNDP 1987). A major fault (74 km length) is identified from the north of Ponneri to Keshavaram running in NE-SW direction (UNDP 1987). Another major fault is inferred running along with the eastern contact between the crystalline and sedimentary formations. Arani and Korttalaiyar rivers for certain distances are aligned along the faults (Rajaveni 2015).

Hydrogeological investigations

The alluvial deposits are characterized by a number of clay lenses and therefore the deposit is divided into two water-bearing layers i.e. clay and sandy clay of approximately 3 to 5 m thickness which extends up to a distance of 30 km west of the coast. The geological cross-section was prepared based on the lithology collected from the CMWSSB. Based on the lithology, field investigation and groundwater head measurement, two aquifers, one unconfined and one semi-confined were identified which had an extent of 30 km from the coast. Beyond this distance, the two aquifers merge and become a single aquifer. Fig. 2b shows semi-confining layer acted like a leaky layer which allows groundwater infiltration from unconfined aquifer to semi-confined aquifer (Rajaveni 2015).

"Insert Figure 2a and 2b"

The dug wells in this area are generally less than 20 m deep and tube wells are up to 120 m deep. The groundwater head in the unconfined aquifer ranges from 2 to 6 m bgl and in the semi-confined aquifer, it ranges from 14 to 20 m bgl. The water from these wells is used for domestic, irrigational and municipal purposes. The six wellfields located in the alluvial deposits and paleo buried channels have 98 pumping wells. Previous studies by Rao et al. (2004b), and Charalambous and Garratt (2009) on the recharge and abstraction relationship in this region were carried out through finite element model only by considering it as a single confined aquifer system. Due to the interaction between the unconfined and semi-confined aquifer during pumping, it is crucial to consider them as two aquifers in the model. In general, the regional groundwater flow is towards the sea; however, there may be variations in local hydraulic heads due to the difference in pumping pattern.

Modelling of groundwater flow and transport

Three-dimensional groundwater flow equation in an unconfined aquifer given by Rushton (2003) is:

$$\frac{\partial}{\partial x}\left(K_x \frac{\partial h}{\partial x}\right) + \frac{\partial}{\partial y}\left(K_y \frac{\partial h}{\partial y}\right) + \frac{\partial}{\partial z}\left(K_z \frac{\partial h}{\partial z}\right) = 0 \quad (1)$$

Where K_x, K_y, and K_z are the hydraulic conductivities (LT^{-1}) along x, y and z-coordinate directions, h is the hydraulic head (L), x_i is the Cartesian co-ordinates (L). Basic Richards equation is written with these two unknown variables in one balance equation. Finite element model based on the Richards equation is written in the following form which has to be solved either for ψ or s (DHI 2009b).

198 $$R(s,\psi) = S_0\, s(\psi)\, \frac{\partial \psi}{\partial t} + \varepsilon \frac{\partial s(\psi)}{\partial t} - \nabla.\{K_r(\psi)K[\nabla\psi+(1+\chi)e]\} - Q = 0 \quad (2)$$

199

200 Where ψ is the pressure head, ($\psi > 0$ saturated medium,
201 $\psi \leq 0$ unsaturated medium), $s(\psi)$ is the saturation, ($0<s\leq1$, $s = 1$ if medium is saturated), t is
202 time, S_0 is the specific storage due to fluid and medium compressibility, ε is porosity, $K_r(\psi)$ is
203 relative hydraulic conductivity ($0<K_r\leq1$, $K_r=1$ if saturated at $s = 1$), K is tensor of hydraulic
204 conductivity for the saturated medium (anisotrophy), χ is buoyancy coefficient including fluid
205 density effects, e is gravitational unit vector, Q is specific mass supply, and R is residual. This
206 equation was used to simulate the spatial and temporal variation in hydraulic head based on
207 flow between the finite-element cells of the model.

208 A generalized form of the solute transport equation is presented by Grove (1976) as

209 $$\frac{\partial(\varepsilon C)}{\partial t} = \frac{\partial}{\partial x_i}\left(\varepsilon D_{ij}\frac{\partial C}{\partial x_j}\right) - \frac{\partial}{\partial x_i}(\varepsilon C V_i) - C'W* + CHEM \quad (3)$$

210

211 Where CHEM = $-\rho_b \partial C/\partial t$ for linear equilibrium-controlled sorption or ion-exchange reactions.
212 D_{ij} is the coefficient of hydrodynamic dispersion, (L^2T^{-1}), C' is the concentration of the
213 groundwater in the source or sink fluid, C is the concentration of the species adsorbed on the
214 solid (mass of solute/mass of solid), ρ_b is the bulk density of the sediment, (ML^{-3}), V_i is the
215 seepage velocity, (LT^{-1}), W* is the volume flux per unit area, (LT^{-1}), and ε is the effective
216 porosity of the porous medium. The first term on the right side of equation (3) represents the
217 change in concentration due to hydrodynamic dispersion. The second term of equation (3)
218 represents advective transport and it describes the movement of solutes at the average seepage
219 velocity of the groundwater flow. The third term of equation (3) represents the effects of mixing
220 with a source fluid that has a different concentration than the groundwater at the location of the
221 recharge or injection. The fourth term of equation (3) lumps all of the chemical, geochemical,

222 and biological reactions that cause transfer of mass between the liquid and solid phases or
223 conversion of dissolved chemical species from one form to another (Konikow 1996).
224
225 Three-dimensional density-dependent mass transport is modelled in Finite Element subsurface
226 FLOW (FEFLOW) on the basis of the Darcy law and nonlinear (non-Fickian) dispersion law
227 (DHI 2009b). In the linear Fickian law, the dispersive mass flux of a solute is proportional to
228 the solute concentration gradient. Density coupled flow and transport processes is simulated
229 by following equations (DHI 2009b)

230 $$\frac{\partial(\varepsilon\rho)}{\partial t} + \nabla.(\rho v) = Q_\rho \quad (4)$$

231 $$\frac{\partial(\varepsilon C)}{\partial t} + \nabla.(Cv + J_C) = Q_C \quad (5)$$

232
233 Where C is the concentration, (ML^{-3}), J_C is Fickian mass flux vector, ($ML^{-2}T^{-1}$), p is fluid
234 pressure, ($ML^{-1}T^{-2}$), Q_ρ is bulk fluid flow sink/source, ($ML^{-3}T^{-1}$), Q_C is bulk mass sink/source,
235 ($ML^{-3}T^{-1}$), v is Darcy velocity vector, (LT^{-1}), α is solute expansion coefficient, (1), ε is
236 porosity,ρ is fluid density, (ML^{-3}), μ is dynamic viscosity of fluid, ($ML^{-1}T^{-2}$).
237
238 In the present study, the coastal alluvial aquifer has complex geometry and boundary
239 conditions. SGD is assessed by three-dimensional numerical groundwater flow simulation
240 software of FEFLOW version 6.2. In this method, the area of interest is divided into various
241 irregular triangular shaped elements. It is possible to refine the size of the elements much
242 smaller along the coastal regions where a better accuracy of SGD should be estimated. The
243 unknown value of groundwater head for the different time periods is computed at the triangle
244 intersect nodes. The groundwater head of the interior of each cell is determined by interpolation
245 between the nodal points.

Model development

Conceptual model development and discretisation

Fig. 1 shows the Arani and Korttalaiyar river basin in which the area considered for the groundwater modelling was delineated based on the geomorphology, geology and hydrogeological conditions. That is, to carry out groundwater modelling, possible aquifer zones with a thickness greater than 10 m were delineated. The north, south and western boundary of this area side was fixed as the watershed boundary. Even though, the Arani river enters the area considered for the groundwater modelling from the northwest, this was demarcated as the aquifer boundary due to the considerable reduction in the width of the alluvium due to the presence of laterite.

This complex two aquifer system was discretized into nine layers considering the lithological variations observed in the area. The model is developed for 90 km from the coast. For about 30 km from the coast, the layer 1 and 2 represent the unconfined aquifer, layer 3 and 4 represent semi-confining layer (aquitard) and layers from 5 to 8 represent the semi-confined aquifer. Beyond 30 km from the coast, the layers from 1 to 8 represent the single unconfined aquifer. Layer 9 represents the bottom of the aquifer which is impermeable. The model area of 1456 km^2 was discretized into finite element mesh consisting of approximately 1.5 million triangular finite element cells (Fig. 3a). The size of the cells initially varies from 0.056 km^2 to 0.424 km^2. The mesh size was further refined along the river course and around the wellfield areas to estimate the head and solute concentration with finer resolution. The size of the finite element cells in these regions varies from 500 m^2 (near well field and river) to 35,000 m^2 (far from well

field and river). Fig. 3b shows the north-south cross-section of the groundwater model. Aquifer thickness includes elevation of the top and bottom of the aquifer which was derived from the borehole logs and from previous studies conducted by UNDP (1987). The elevation of the top of the aquifer ranges from 0 m to 133 m msl (mean sea level).

"Insert Figure 3a and 3b"

Boundary and initial conditions

The eastern side of the area bounded by the Bay of Bengal was considered as a constant head boundary. The northern and southern boundaries are watershed boundaries; they were considered as no-flow conditions. The Palar river is flowing on the southwestern side and hence it is a variable head. The two rivers flowing in this region were considered as river head boundary. To determine the initial groundwater head, the monthly groundwater level data available for 47 wells (Fig. 1) from the year 1990 to 2010 was analyzed. The groundwater head measured during January 1996 was considered as an initial head because it is identified that seawater intrusion during January 1996 was very low with the groundwater head in both the aquifers was zero m msl at the coast.

Aquifer Parameters

Aquifer parameters such as hydraulic conductivity, porosity and specific yield were assigned to each element based on pumping test data (UNDP 1987). The specific yield of the aquifers was obtained from Todd (2001) and Fetter (2001) for different formations. The range of values of aquifer parameters considered for modelling is given in Table 2. The hydraulic conductivity values from the twenty pumping tests were extrapolated to the area around them by the Thiessen polygon method. This method was preferred over contouring due to the shortage of

296 data points. The hydraulic conductivity of the unconfined aquifer varies from 35 m/day to 100
297 m/day and for aquitard, it varies from 0.001 to 0.01 (UNDP 1987, TNPWD 2012). Hydraulic
298 conductivity of the semi-confined aquifer (sandy aquifer) varies from 100 m/day to 250 m/day
299 (UNDP 1987, TNPWD 2012). The hydraulic conductivity and the thickness of the semi-
300 confined aquifer is higher compared to the unconfined aquifer. The porosity of the aquifer was
301 found in between 0.15 to 0.20 (UNDP 1987). Specific storage values were calculated from the
302 aquifer thickness and storativity which ranges from 0.004 to 0.0009 (Todd 2001, Fetter 2001).
303
304 ***Groundwater recharge and abstraction***
305 Analysis of the relation between rainfall and groundwater head is one of the methods for
306 estimating groundwater recharge. Rainfall data from 9 raingauge stations were compared with
307 the groundwater head from the monitoring wells located in the unconfined aquifer. The
308 monthly variation in rainfall and groundwater head in the unconfined aquifer from 1996 to
309 2012 shows the immediate rise in groundwater head after rainfall (Fig. 4). The rise in
310 groundwater head is about 8 m when the monthly rainfall exceeds 500 mm. The specific yield
311 of the unconfined aquifer is considered to be 15 percent of rainfall in comparison with the
312 groundwater head. Even though, this is an approximate method of estimation of groundwater
313 recharge, the percentage of rainfall recharge determined is comparable with the estimate for
314 this area given by the Groundwater Resources Estimation Committee (GEC 1997).
315
316 The variation in groundwater recharge was applied based on the geology and the
317 location of rain gauge stations. The area was divided into 9 Thiessen polygons to define
318 monthly groundwater recharge. Based on the previous studies (Charalambous and Garratt
319 2009, Anuthaman 2009, GEC 1997) norms, the groundwater recharge was assigned from 10%
320 to 20%. A return flow from the agricultural field also provides groundwater recharge.

Charalambous & Garratt (2009) and Anuthaman (2009) stated that almost 39% of irrigation water used in this region returns to the aquifer. Hence, 39 % of pumped water was considered as irrigation return flow. Arani and Korttalaiyar rivers flow only for a few days during the northeast monsoon season (October to December) and the river stage were assigned for river head boundaries.

"Insert Figure 4"

The indirect method of crop water requirement method was adopted to calculate the groundwater pumping. Advanced techniques of remote sensing and GIS (IRS 1D LISS-III imageries) were applied to prepare land use maps for different seasons. The crop water requirement was estimated from this land use. Groundwater pumping was calculated by multiplying the water requirements of each crop with its corresponding area. The land area was classified into 6 categories such as agriculture, built-up, forest, water bodies, wasteland and wetland.

Results and discussion

Model calibration and validation

FEFLOW model was developed to simulate the temporal variation of discharge of submarine groundwater across the seafloor. This model is capable of solving three-dimensional density-dependent flow patterns and recirculated seawater near the seashore and is used to calculate the rate and direction of movement of groundwater through aquifers. The outputs from the model simulation provide information about hydraulic heads and SGD rates for specified hydrogeological conditions. The accuracy of the developed model mainly depends on the availability of exact field data which represents the real world. In order to obtain a reasonably

accurate representation of field condition, the model was calibrated in steady and transient state conditions.

Steady-state calibration was done by adjusting aquifer parameters within the reported range until the model reproduces observed data close enough. Several trial runs were made to minimize the difference between the observed and the simulated groundwater head. After several runs, the best possible match between the observed and simulated head was achieved when the R^2 values for regression line drawn between the two for unconfined and semi-confined aquifer were 0.990 and 0.901 respectively (Fig. 5a and 5b). Then, transient data collected from groundwater recharge and pumping were applied in the FEFLOW model to simulate transient state calibration. Transient state calibration was carried out from January 1996 to December 2003. Transient state calibration was made until the best possible match was obtained between observed and simulated groundwater heads. After the transient state calibration, the R^2 values for the regression line were 0.993 and 0.901 between the observed and simulated heads in the unconfined and semi-confined aquifers respectively (Fig. 5c and d). After successful calibration of steady and transient state, validation of the model was carried out by comparing the simulated groundwater head with the observed heads from January 2004 to December 2012 with the input parameters derived from calibration.

"Insert Figure 5a and 5b"

Flow Simulation

In order to visualize the impact of over-pumping of this aquifer, a west to the east cross-section from Kannigaipper to the coast, approximately at the center of the aquifer was prepared. The simulated groundwater head in the unconfined and semi-confined aquifers with respect to distance from the sea during January and June for the years 2000, 2005 and 2010 are shown in

Fig. 6a and 6b. The severe decline in groundwater head to the level of around −35 m msl was noted in the year 2005. This was due to a reduction in recharge as a consequence of low rainfall in the years 2002, 2003 and 2004. This led the groundwater pumped from wells that supply water to the Chennai city become saline. Hence, the groundwater pumping from the Minjur and Panjetti well fields that supply water to the city was stopped in the year 2005. As a result of the termination of pumping from these well fields in 2005, the groundwater head started to increase, and it is noticed in the year 2010 (Fig. 6a and 6b).

"Insert Figure 6a and 6b"

The total rate of discharge of fresh submarine groundwater along the eastern boundary of the study area from January 1996 to December 2018 in the unconfined and semi-confined aquifers are shown in Fig. 7a and b. Positive values indicate saltwater intrusion and negative values indicates SGD. In the unconfined aquifer, the fresh groundwater was found to be continuously discharged to the sea and the total SGD to the sea was higher during December. That is, a higher amount (of about 60,000 m^3/day) of fresh groundwater discharged into sea in post-monsoon compared to the pre-monsoon in the unconfined aquifer. The fresh SGD to the sea is reduced after 2004, Tsunami and it is gradually increased after 2005 flood in this study area. There is a huge increase in fresh SGD in January 2016 because of severe flooding (Gowrisankar et al. 2017) after that it gradually reduced. However, in the semi-confined aquifer, the seawater (positive values) is intruding into the freshwater aquifer due to the over-pumping of groundwater from well fields. The discharge from the sea was comparatively lesser in January than in June. There is a sudden decrease of seawater to the aquifer from the year 1996 to 1998 because the number of check dams constructed since then had increased.

"Insert Figure 7a and 7b"

394 The fresh SGD along the eastern boundary of the model area from the unconfined and semi-
395 confined aquifers for the months of January and June for the years 2000, 2005 and 2010 are
396 shown in Fig. 8a and b. In the unconfined aquifer, the rate of fresh SGD to the sea is high
397 during January (post-monsoon) than June (pre-monsoon). However, in the semi-confined
398 aquifer, the saline SGD is always moving towards the aquifer. During January, the inflow from
399 the sea is comparatively lesser than in June. In the year 2005, the rate of seawater intruded into
400 the lower aquifer was very high (Fig. 8b).
401
402 *"Insert Figure 8a and 8b"*
403
404 **Prediction of Submarine Groundwater Discharge**
405 ***Baseline scenario***
406 The baseline scenario is introduced to determine the rate of SGD in the future by assuming
407 annual pumping and recharge will remain constant. This scenario will be helpful to suggest the
408 response of the aquifer and the amount of SGD can be calculated for the long-term if the present
409 condition exists. As explained earlier, the negative values in Fig. 9a indicate fresh SGD.
410 Temporal variation of the SGD rate along the upper aquifer is shown in Fig. 9a. In the
411 unconfined aquifer, the graph shows an increasing trend of fresh SGD for 2030 and the seasonal
412 fluctuation depends on the tendency of the rainfall. Fresh groundwater was predicted to be
413 continuously discharging into the sea. Amount of fresh SGD was greater for the monsoon
414 months (December and January) compared to the summer months (April and May). The
415 simulated results show that the rate of fresh SGD increase by about 43,918 m^3/day during
416 January 2020 and raises to about 61,790 m^3/day during December 2030. If the present
417 conditions of rainfall recharge and pumping continue in the future, the rate of fresh SGD will
418 increase from 13,459 m^3/day (April 2020) to 14,010 m^3/day (April 2030) during summer. In

419 the semi-confined aquifer, the baseline scenario shows positive values (Fig. 9b) indicating the
420 seawater movement seawater into the aquifer. This can be reduced from 94,126 m^3/day (Jan
421 2020) to 82,505.5 m^3/day (Jan 2030). It shows a decreasing trend of about 11,418 m^3/day from
422 May 2020 to May 2030. Hence, this baseline scenario itself shows a higher amount of fresh
423 SGD moving into the sea in the unconfined aquifer.
424
425 ***Scenario 1***
426 Climate change predictions indicate a standard deviation of about 130 mm in the projected
427 rainfall in the year 2030 (INCCA 2010), which is about 10% of the present annual rainfall of
428 1,200 mm. For the projected climate change in the northern parts of Tamil Nadu where the
429 study area is located, the rainfall is likely to increase and the water yield to rise by 10% to 40%
430 (INCCA 2010). Hence, scenario 1 was carried out with 10% increase in rainfall recharge and
431 by continuing the same annual pumping rate. Scenario 1 results also follow a similar trend of
432 rainfall as the baseline scenario (Fig. 9a). In the unconfined aquifer, the rate of fresh SGD
433 increases at an average of about 125% when compared to the baseline scenario. In the semi-
434 confined aquifer, the rate of recirculated seawater SGD decreases by an average of about 40%
435 when compared to the baseline scenario. The percentage of fresh SGD rise is greater in the
436 unconfined aquifer compared to the semi-confined aquifer since rainfall exerts higher influence
437 in the unconfined aquifer. In this same aquifer, the groundwater head was rises by about 2 m
438 in both the aquifer for 10% increase in rainfall recharge (Rajaveni et al. 2016), which clearly
439 explains the rate of increase of fresh SGD by scenario 1.
440
441 ***Scenario 2***
442 Over-pumping of groundwater in this region is experienced over the years to meet the water
443 supply demands of Chennai city (CGWB 2007). The Government is resorting to hiring the

444 wells owned by farmers in the region to meet the severe water demand in Chennai city over
445 the years (Meijer 2012). The overexploitation of coastal groundwater leads to both submarine
446 groundwater discharge reduction, as well as an increase of seawater inflow and, consequently,
447 an increase of the transition zone thickness (Custodio 2002). Thus, it is essential to understand
448 the changes in SGD with increase in pumping along with the assumed measures to improve the
449 rainfall recharge. Thus, scenario 2 was carried out with 10 % increase in pumping and
450 implementation of managed aquifer recharge (MAR) (with additional check dams, 1 m increase
451 in crest level of all the existing check dams, rehabilitation of lakes and ponds, and interlinking
452 of Arani and Korttalaiyar rivers) structures in addition to same annual rainfall recharge as in
453 the scenario. Temporal distribution of SGD along the shoreline from January 2020 to
454 December 2030 is shown in Figure 9a and 9b. Comparing this distribution with the baseline
455 scenario, the fresh SGD rate in the unconfined aquifer increases by around 116 %, lower than
456 scenario 1. In the semi-confined aquifer, the recirculated seawater SGD rate decreases by about
457 91 % compared to the baseline scenario, and it increases by around 260% compared to scenario
458 1. This is because of a 10% increase in groundwater pumping.
459
460 ***Scenario 3***
461 Scenario 2 represents the increase in pumping which may adversely affect the aquifer by
462 seawater intrusion. Appropriate and well-organized management is essential to avoid further
463 ingress of seawater intrusion due to over-extraction and to enhance the groundwater quality.
464 Hence, the effect of decrease in groundwater pumping by 10% was simulated with the assumed
465 MAR structures to improve the groundwater recharge, and following the same annual rainfall
466 recharge i.e. how much %. By comparing scenario 3 with the baseline, the rate of fresh SGD
467 rises by an average of about 140% in the unconfined aquifer and the rate of recirculated
468 seawater SGD reduced by an average of about 24% in the semi-confined aquifer. Comparing

scenario 3 with scenario 2 indicates greater positive impacts in fresh SGD in the unconfined aquifer and reduction of about 27% of recirculated seawater SGD towards an inland aquifer. This scenario also follows similar trends of fresh and seawater SGD like scenario 1 and 2. The reduction in groundwater pumping helps to stop seawater intrusion in the semi-confined aquifer and replenish a greater amount of fresh SGD towards the sea in the unconfined aquifer.

Scenario 4

In order to assess the combined aspect of MAR structures, pumping and rainfall recharge on groundwater head, all these scenarios were combined and the SGD rate was predicted. Scenario 4 was carried out with MAR structures, 10% increase in rainfall recharge, and termination of pumping from five wellfields. In the unconfined aquifer, the fresh SGD rate has increased at an average of 173% and 123% compared to baseline and scenario 3 respectively. Implementation of scenario 4 can help to improve the groundwater quality for a long time. In the semi-confined aquifer, the simulated results show decreasing trend of recirculated seawater SGD i.e. saline water is changed into freshwater (negative values in Fig. 9b) during the monsoon from October to January. Comparing the results of scenario 4 with the baseline show that the rate of seawater SGD is reduced by about 80500 m^3/day during the pre-monsoon i.e. June and about 83200 m^3/day during the post-monsoon i.e. Thus, the implementation of MAR structures enhances the fresh SGD rate during non-monsoon months also, increases base flow. MAR structures provide to maintain the greater groundwater head level and helping to improve base flow during low flow periods. Salameh et al. (2019) also reported the MAR structures can improve the influence of climatic changes on the availability of water in arid and semi-arid areas by increasing the stored amounts of groundwater and the effects of a decrease of seawater intrusion. Hence, the integrated MAR structures, increase in rainfall recharge, and reduction in pumping completely pushes back the freshwater – seawater interface towards the sea and solves

494 the seawater intrusion problem during monsoon months. The flow budget for all the scenarios
495 during January 2030 and June 2030 are given in Tables 3 and 4 respectively. This table
496 indicates that the fresh SGD rate to the sea increased by the implementation of measures
497 considered in scenario 4. Fresh SGD discharge is widely used as a water resource for drinking,
498 hygiene, agriculture, fishing, tourism, culture, or ship navigation. In Peru, fresh SGD is used
499 for drinking, on Tahiti for bathing, in Greece for irrigation (Moosdorf and Oehler 2017). In
500 order to restore this coastal aquifer and for sustainable management of water resources, it is
501 essential to adopt measures as suggested in scenario 4.

502 *"Insert Figure 9a and 9b"*

503

504 ## Conclusion

505 Exchange of submarine flow of water between the sea and aquifer were assessed in the Arani-
506 Korttalaiyar river basin, north of Chennai, India, by finite element modelling. The rate of
507 movement of seawater to the aquifer has increased from 17,000 m^3/day to 24,500 m^3/day due
508 to the over-exploitation of groundwater from the semi-confined aquifer. The finite element
509 model was used to predict the effect of recharge structures i.e. with additional check dams, 1
510 m increase in crest level of all the existing check dams, interlinking of rivers, 10% increase in
511 rainfall recharge and termination of pumping from five wellfields. By adopting all possible
512 pumping and recharge methods, seawater moving towards fresh water aquifer (rate of 4,408
513 m^3/day) can be significantly reduced and fresh SGD (rate of 22,414 m^3/day) rate increased.
514 Thus, the three-dimensional numerical model was successfully used as a tool to quantify the
515 impact of over-exploitation on fresh SGD rates under different scenarios. The insights from
516 this study will be useful for fresh water and saline water management in the coastal areas.

517

518
519

520 **Declaration**

521

522 Ethics approval and consent to participate - NO

523

524 Consent for publication - NO

525

526 Availability of data and materials - The groundwater level, rainfall and pumping datasets
527 generated and/or analyzed during the current study are collected from PWD, CGWB and Metro
528 water department

529

530 Competing interests - The authors declare that they have no competing interests

531

532 Funding - Funding from the Department of Science and Technology, New Delhi, India (Grant
533 number: DST/WAR-W/SWI/05/2010). Co-funding from the European Commission within the
534 Seventh Framework Programme (Grant number: 282911)

535

536 Authors' contributions - SPR conceptualized and developed the numerical groundwater flow
537 model and interpreted results. ISN collected data of groundwater level. KB interpreted results
538 of groundwater head. LE conceptualized the idea of this study. All authors were involved in
539 writing and approval of the final manuscript.

540

541 Acknowledgements - Funding from the Department of Science and Technology, New Delhi,
542 India (Grant number: DST/WAR-W/SWI/05/2010) is acknowledged. Co-funding for the
543 collaborative project ‘Enhancement of natural water systems and treatment methods for safe
544 and sustainable water supply in India – SaphPani’ (www.saphpani.eu) from the European
545 Commission within the Seventh Framework Programme (Grant number: 282911) is gratefully
546 acknowledged. The authors thank the Tamil Nadu Public Works Department and the Chennai
547 Metropolitan Water Supply and Sewerage Board, India, for providing the necessary
548 groundwater level and borehole data. Authors greatly acknowledge DHI WASY for providing
549 FEFLOW license.

550

551

552

553 **References**

554 Anuthaman NG (2009) Groundwater augmentation by flood mitigation in Chennai region, a
555 modelling based study. Ph.D. thesis. Anna University Chennai, India

556 Babu DSS, Anish M, Vivekanandan KL, Ramanujam N, Murugan KN, Ravindran AA (2009)
557 An Account of Submarine Groundwater Discharge from the SW Indian Coastal Zone.
558 Journal of Coastal Research 25(1): 91- 104

559 Basu AR, Jacobsen SB, Poreda RJ, Dowling CB, Aggarwal PK (2001) Large groundwater
560 strontium flux to the oceans from the Bengal Basin and the marine strontium isotope
561 record. Science 293: 1470–1473

562 Biswas H, Sena DR, Kumar G, Lakaria BL, Raizada A, Kumar S, Mishra PK (2017) Effect of
563 water storage structures on groundwater recharge in India. Groundwater for Sustainable
564 Development 4: 49–56

565 Bobba AG (2011) Simulation of Groundwater and Contamination Discharge from Krishna –
566 Godavari Coast to Bay of Bengal, India

567 Bokuniewicz H, Buddemeier R, Maxwell B, Smith C (2003) The typological approach to
568 submarine ground-water discharge (SGD). Biogeochemistry 66: 145–158

569 CGWB 2007, District ground water brochure Tiruvallur district

570 Chakrabarti R, Mondal S, Acharya SS, Lekha JS, Sengupta D (2018) Submarine groundwater
571 discharge derived strontium from the Bengal Basin traced in Bay of Bengal water samples.
572 Nature. Scientific Reports 8: 4383

573 Charalambous AN, Garratt P (2009) Recharge–abstraction relationships and sustainable yield
574 in the Arani–Kortalaiyar groundwater basin, India. Quarterly Journal of Engineering
575 Geology and Hydrogeology 42: 39-50

576 Chidambaram S, Nepolian M, Ramanathan AL et al (2017) An attempt to identify and estimate
577 the subsurface groundwater discharge in the south-east coast of India. International Journal

578 of Sustainable Built Environment 6: 421–433
579 Custodio, E. (2002) Aquifer Overexploitation: What Does It Mean? Hydrogeol. J. 10: 254–277
580 Debnath P, Das K, Mukherjee A, Ghosh NC, Rao S, Kumar S, Krishan G, Joshi G (2019)
581 Seasonal-to-diurnal scale isotopic signatures of tidally-influenced submarine groundwater
582 discharge to the Bay of Bengal: Control of hydrological cycle on tropical oceans. Journal
583 of Hydrology 571: 697-710
584 Debnath P, Mukherjee A (2016) Quantification of tidally-influenced seasonal groundwater
585 discharge to the Bay of Bengal by seepage meter study. Journal of Hydrology 537: 106 –
586 116
587 Debnath P, Mukherjee A, Das K (2018) Characterization of tidally-influenced seasonal nutrient
588 flux to the Bay of Bengal and its implications on the coastal ecosystem. Hydrological
589 Processes. DOI: 10.1002/hyp.11507
590 Debnath P, Mukherjee A, Singh HK, Mondal S (2015) Delineating seasonal porewater
591 displacement on a tidal flat in the Bay of Bengal by thermal signature: Implications for
592 submarine groundwater discharge. Journal of Hydrology 529: 1185-1197
593 DHI (2009b) Finite element subsurface flow and transport simulation. White paper vol.
594 Fetter CW (2001) Applied Hydrogeology. 4th Edition, Prentice - Hall in, Upper Saddle river,
595 NJ
596 Finkl CW, Krupa SL (2003) Environmental impacts of coastal-plain activities on sandy beach
597 systems: hazards, perception and mitigation. J. Coastal Res. 35: 132–150
598 GEC (1997) Groundwater Resource Estimation Methodology. Report of the Groundwater
599 Resource Estimation Committee, Ministry of Water Resources, Government of India
600 George ME, Babu DSS, Akhil T, Rafeeque MK (2018) Investigation on Submarine
601 Groundwater Discharge at Kozhikkode Coastal Aquifer, SW Western Ghats. Journal
602 Geological Society of India 92: 626-633

603 Gowrisankar G, Chelliah R, Ramakrishnan SR, Elumalai V, Dhanamadhavan S, Brindha K,
604 Antony U, Elango L (2017) Chemical, microbial and antibiotic susceptibility analyses of
605 groundwater after a major flood event in Chennai. Sci Data. 4: 170135
606 Grove DB (1976) Ion exchange reactions important in groundwater quality model. Advances
607 in Groundwater Hydrology 409-436
608 INCCA (2010) Climate change and India: A 4x4 assessment a sectoral and regional analysis
609 for 2030's
610 Jacob N, Babu DSS, Shivanna K (2009) Radon as an indicator of submarine groundwater
611 discharge in coastal regions. Current Science 97(9): 1313-1320
612 Konikow LF (1996) Numerical models of groundwater flow and transport. In: Manual on
613 Mathematical Models in Isotope Hydrogeology. International Atomic Energy Agency
614 Report: 59-112
615 Kourakos G, Dahlke HE, Harter T (2019). Increasing groundwater availability and seasonal
616 base flow through agricultural managed aquifer recharge in an irrigated basin. Water
617 Resources Research 55: 7464–7492
618 Krishan G, Rao MS, Kumar CP, Kumar S, Rao MRA (2015) A study on identification of
619 submarine groundwater discharge in northern east coast of India. Aquatic Procedia 4: 3 –
620 10
621 Kwon EY, Kim G, Primeau F, Moore WS, Cho HM, DeVries T, Sarmiento JL, Charette MA,
622 and Cho YK (2014) Global estimate of submarine groundwater discharge based on an
623 observationally constrained radium isotope model. AGU, Geophysical Research Letters
624 10.1002/2014GL061574
625 Langevin CD (2003) Simulation of submarine groundwater discharge to a marine estuary:
626 Biscayne Bay, Florida. Ground Water 41(6): 758–771
627 Luijendijk E, Gleeson T, Moosdorf N (2020) Fresh groundwater discharge insignificant for the

628 world's oceans but important for coastal ecosystems. Nature Commun. 11: 1260
629 Manivannan V, Elango L (2019) Seawater intrusion and submarine groundwater discharge
630 along the Indian coast. Environmental Science and Pollution Research.
631 https://doi.org/10.1007/s11356-019-06103-z
632 Meijer P (2012) Case study on extraction of groundwater in the A-K basin in the north of
633 Chennai, India. Master Thesis. Wageningen University
634 Moosdorf, Oehler (2017). Societal use of fresh submarine groundwater discharge: An
635 overlooked water resource. Earth-Science Reviews 171: 338–348
636 Pathak S (2019) No Drips, No Drops: A City Of 10 Million Is Running Out Of Water
637 Prakash R, Srinivasamoorthy K, Gopinath S, Saravanan K (2018) Measurement of submarine
638 groundwater discharge using diverse methods in Coleroon Estuary, Tamil Nadu, India.
639 Applied Water Science 8: 13
640 Rahaman W, Singh SK (2012) Sr and $^{87}Sr/^{86}Sr$ in estuaries of western India: Impact of
641 submarine groundwater discharge. Geochimica et Cosmochimica Acta 85: 275–288
642 Rajaveni SP (2015) Integrated approach of modelling of runoff, infiltration and density
643 dependent groundwater flow: A case study in seawater intruded coastal aquifer north of
644 Chennai, India. Ph.D. thesis, Anna University Chennai, India
645 Rajaveni SP, Indu SN, Elango L (2016) Finite element modelling of a heavily exploited coastal
646 aquifer for assessing the response of groundwater level to the changes in pumping and
647 rainfall variation due to climate change. Hydrology Research 47(1): 42-60
648 Rao SVN, Saheb SM, Ramasastri KS (2004b) Aquifer restoration from seawater intrusion: a
649 preliminary field scale study of the Minjur aquifer system, north of Chennai, Tamil Nadu,
650 India, Proceedings of 18th Seawater Intrusion Meeting Cartagena, Spain: 707 - 715
651 Ravindran AA, Ramanujam N (2014) Detection of submarine groundwater discharge to coastal
652 zone study using 2D electrical resistivity imaging study at Manapad, Tuticorin, India.

653 Indian Journal of Geo-Marine Sciences 43(2): 224-228
654 Rengarajan R, Sarma VVSS (2015) Submarine groundwater discharge and nutrient addition to
655 the coastal zone of the Godavari estuary. Marine Chemistry 172: 57–69
656 Rushton KR (2003) Groundwater Hydrology: Conceptual and Computational Models. Wiley
657 Published 430
658 Salameh E, Abdallat G, Valk MVD (2019) Planning Considerations of Managed Aquifer
659 Recharge (MAR) Projects in Jordan. Water 11: 182
660 Srinivasamoorthy K, Ponnumani G, Prakash R, Gopinath S, Saravanan K, Vinnarasi F (2018)
661 Tracing groundwater inputs to Bay of Bengal from Sankarabarani River Basin,
662 Pondicherry, India, using continuous radon monitoring. Int J Environ Sci Technol
663 Taniguchi M, Burnett WC, Cable JE, Jeffrey V, Turner (2002) Investigation of submarine
664 groundwater discharge. Hydrol. Process 16: 2115–2129
665 Taniguchi M, Dulai H, Burnett KM, Santos IR, Sugimoto R, Stieglitz T, Kim G, Moosdorf N,
666 Burnett WC (2019) Submarine Groundwater Discharge: Updates on Its Measurement
667 Techniques, Geophysical Drivers, Magnitudes, and Effects, Frontiers in Environmental
668 science 7:141
669 TNPWD (2012). Thiruvallur district report, Government of Tamil Nadu
670 Todd DK (2001) Groundwater Hydrology. 2nd Edition, John wiley & Sons, New York
671 UNDP (1987) Hydrogeological and artificial recharge studies Madras, Technical report, United
672 Nations Department of technical co-operation for development, New York, USA
673 Vollberg F, Walther M, Gärdes A, Moosdor N (2019) Modeling the Potential of Submarine
674 Groundwater Discharge to Facilitate Growth of Vibrio cholerae Bacteria. Hydrology 6: 39
675 Virtasalo JJ, Schröder JF, Luoma S, Majaniemi J, Mursu J, Scholten J (2019) Submarine
676 groundwater discharge site in the First Salpausselkä ice-marginal formation, south
677 Finland. Solid Earth 10: 405-423

678 Welch E M, Dulai H, El-Kadi A, Shuler C K (2019) Submarine Groundwater Discharge and
679 Stream Baseflow Sustain Pesticide and Nutrient Fluxes in Faga'alu Bay, American Samoa.
680 Front. Environ
681 Yadav VB, Jha SK, Pulhani V, Tripathi RM (2019) Estimation of submarine groundwater
682 discharge using radium mass-balance in Mumbai Harbour Bay, Mumbai, India. J
683 Radioanal Nucl Chem. 319(3): 945– 952
684
685
686
687
688
689
690
691
692
693
694
695
696
697
698
699
700
701
702

703

704 **List of Tables**

709

710

711

712

713

714

715

716

717

718

719

720

721

722

723

724

725

726

727

728

729 **List of Figures**

746

747

748

749

750

751

752

753

754 **Table 1** SGD studies carried out along the Indian coast

Location	Method	SGD	Reference
Bengal basin	$^{87}Sr/^{86}Sr$ ratio	0.2 x10^{15} litre/year	Basu et al. (2001)
Vizhinjam, Kerala	Groundwater modelling	10.9 ± 6.1 cm/day.	Babu et al. (2009)
Vizhinjam, Kerala	Radium and radon isotopes	10.9 ± 6.1 cm/day	Jacob et al. (2009)
Krishna –Godavari Coast	Dupuit Ghyben Herzberg model and Darcy's law	0.752 m^3/day	Bobba (2011)
Narmada estuary	The inverse model used to identify Sr concentration, the $^{87}Sr/^{86}Sr$ ratio	5 cm/day during pre-monsoon 280 cm/day during monsoon	Rahaman and Singh (2012)
Manapad, Tuticorin	2D electrical resistivity imaging and Darcy law	0.020 m^3/day, 0.006 m^3/day and 0.091 m^3/day	Ravindran and Ramanujam (2014)
Chandipur	Temperature and chemical profiling	1.16 x 10^7 m^3/y	Debnath et al. (2015)
Godavari estuary	1.Three end-member mixing model 2.Radium mass balance approach	6.8 to 12.7 × 10^6 m^3/d 1.55 to 7.44 × 10^6 m^3/d and 1.34 to 5.60 × 10^6 m^3/d	Rengarajan and Sarma (2015)
Bengal basin	^{222}Rn measurement of groundwater sample	Identified SGD location through ^{222}Rn	Krishan et al. (2015)
Chandipur	Seepage meter and Cluster experiment	8.98 ± 0.6 x 10^8 m^3/y	Debnath and Mukherjee (2016)
Cuddalore region	Radon, EC concentration and tide	37.24–79.16 cm/day	Chidambaram et al. (2017)
Basin to the Bay of Bengal	Calculating strontium (Sr) flux	Identified SGD locations	Chakrabarti et al. (2018)
Coleroon estuary (Tributary of Cauvery river)	1.Water budget, 2.Darcy law 3.Manual seepage meter	6.9 × 10^6 and 3.2 × 10^3 m^3/yr to 308.3 × 10^3 m^3/yr	Prakash et al. (2018)
Kozhikkode coast	1.Water table elevation surveys 2. in situ hydrochemical 3. Resistivity surveys	Flow path of the groundwater discharge is located	George et al. (2018)
Sankarabarani river basin	Radon mass balance model	0.88 m/day	Srinivasamoorthy et al. (2018)
Chandipur	Stable isotopic and chemical studies	High-resolution, temporally-variable, stable isotope patterns of SGD is studied	Debnath et al. (2019)
Mumbai Harbour Bay	Ra isotopes (Ra and Ra) mass balance method	33.4 × 10^9 lit/day and 64.9 × 10^9 lit/ day	Yadav et al. (2019)
Indian coast	Analysis of groundwater level	Identified the location	Manivannan and Elango (2019)

Table 2 Aquifer parameters used in the model

Aquifer type, thickness	Parameter	Value	Units	Source
Unconfined , 10 m to 15 m	Hydraulic conductivity, K_x & K_y	35 to 100	(m/day)	UNDP (1987) & TNPWD 2012
	Hydraulic conductivity, K_z	3.5 to 10	(m/day)	UNDP (1987) & TNPWD 2012
	Porosity	0.15 to 0.20		UNDP (1987)
	Specific yield	0.025 to 0.33		Todd (2001) & Fetter (2001)
Aquitard, 3 m to 5 m	Hydraulic conductivity, K_x & K_y	0.001 to 0.01	(m/day)	UNDP (1987) & TNPWD 2012
	Hydraulic conductivity, K_z	0.0001 to 0.001	(m/day)	UNDP (1987) & TNPWD 2012
	Porosity	0.15 to 0.20		UNDP (1987) & TNPWD 2012
	Specific yield	0.1		Todd (2001) & Fetter (2001)
Semi-confined, 20 m to 25 m	Hydraulic conductivity, K_x & K_y	100 to 250	(m/day)	UNDP (1987) & TNPWD 2012
	Hydraulic conductivity, K_z	10 to 25	(m/day)	UNDP (1987) & TNPWD 2012
	Porosity	0.15 to 0.20		UNDP (1987) & TNPWD 2012
	Specific yield	0.2		Todd (2001) & Fetter (2001)

769

770 **Table 3** Rate of SGD for all the scenarios during January 2030 (m^3)

S. No.	Scenario	Recharge		Abstraction		Lateral inflow	Lateral outflow
		River recharge	Rainfall recharge	Crop	Well field		
1	Baseline scenario	1603500	262360	1377500	48011	2232220	2672569
2	Scenario 1	1300175	288596	1377500	48011	1837515	2000775
3	Scenario 2	1816513	262360	1515250	52812	2316015	2826826
4	Scenario 3	1684750	262360	1239750	43210	2911830	3575980
5	Scenario 4	1417159	288596	1377500	9035	3538664	3857884

771

772

773

774

775

776

777

778

779

780

781

782

783

784

785

786 **Table 4** Rate of SGD for all the scenarios during June 2030 (m^3)

S. No.	Scenario	Recharge		Abstraction		Lateral inflow	Lateral outflow
		River recharge	Rainfall recharge	Crop	Well field		
1	Baseline scenario	688240	1829700	2283500	56975	2256110	2433575
2	Scenario 1	705702	2012670	2283500	56975	1654961	2032858
3	Scenario 2	1044162	1829700	2511850	62673	1964809	2264148
4	Scenario 3	983641	1829700	2055150	51278	2426585	3133498
5	Scenario 4	718729	2011923	2283500	11505	2882739	3318386

787

788

789

790

791

792

793

794

795

796

797

798

799

800

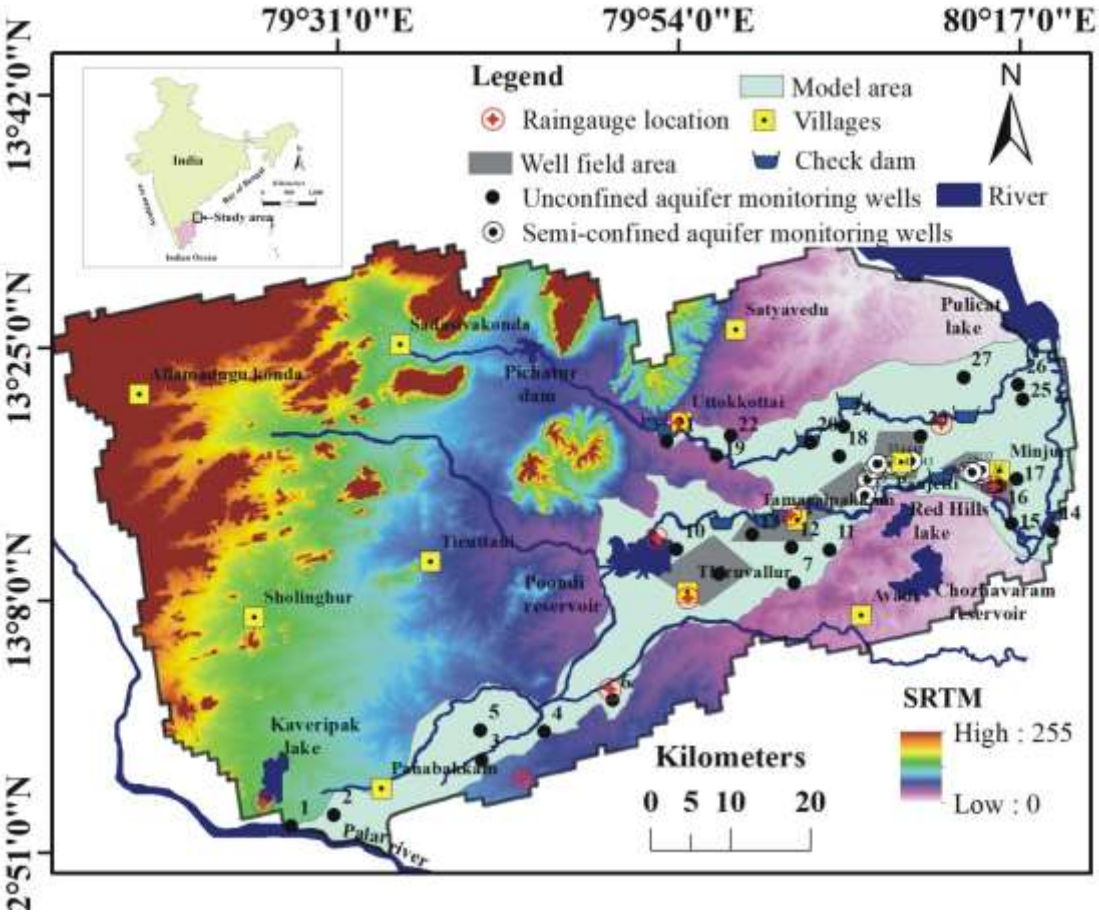

Fig. 1 Location of the study area

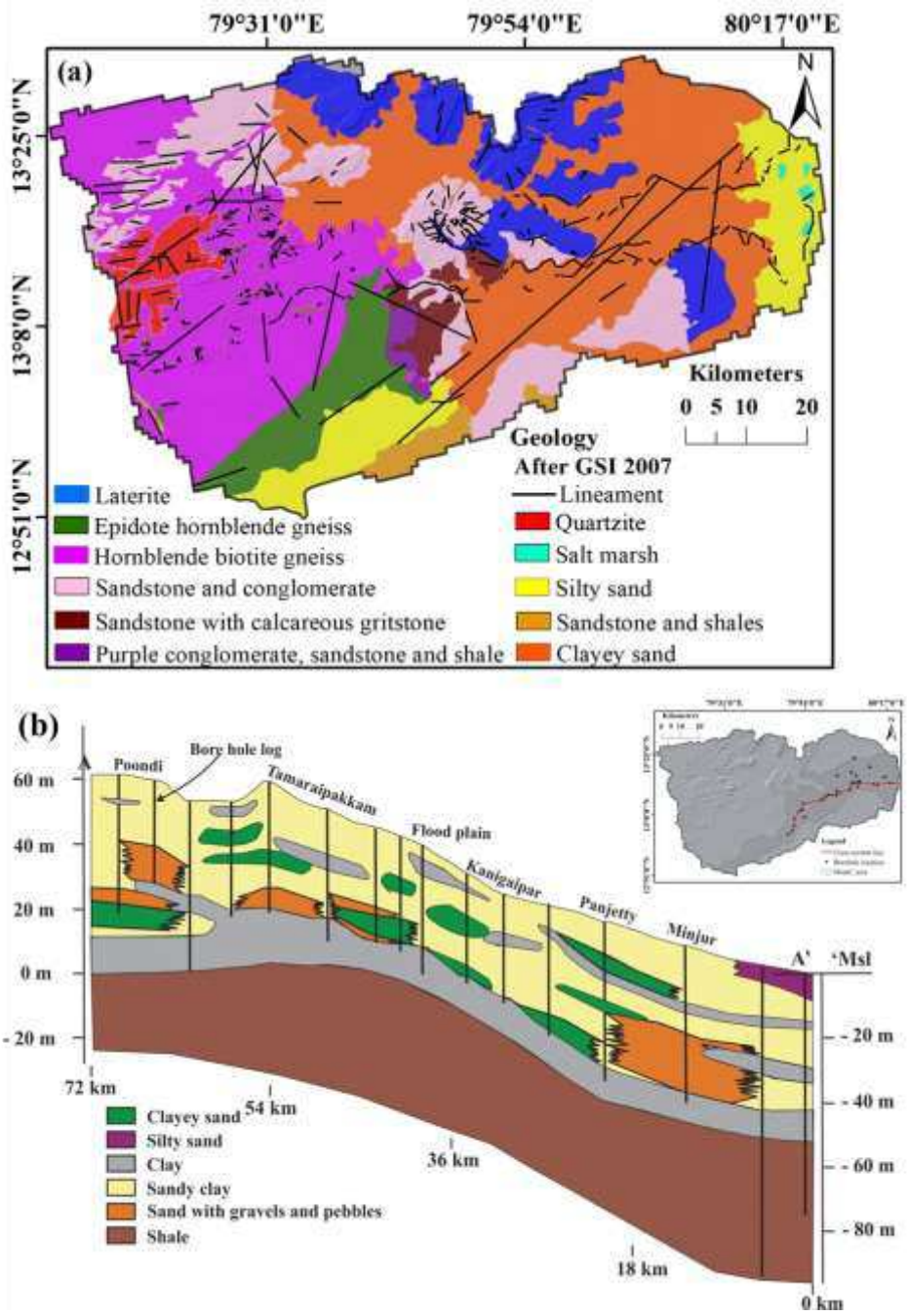

Fig. 2 (a) Geology of the study area **(b)** West to east geological cross section along A-A'

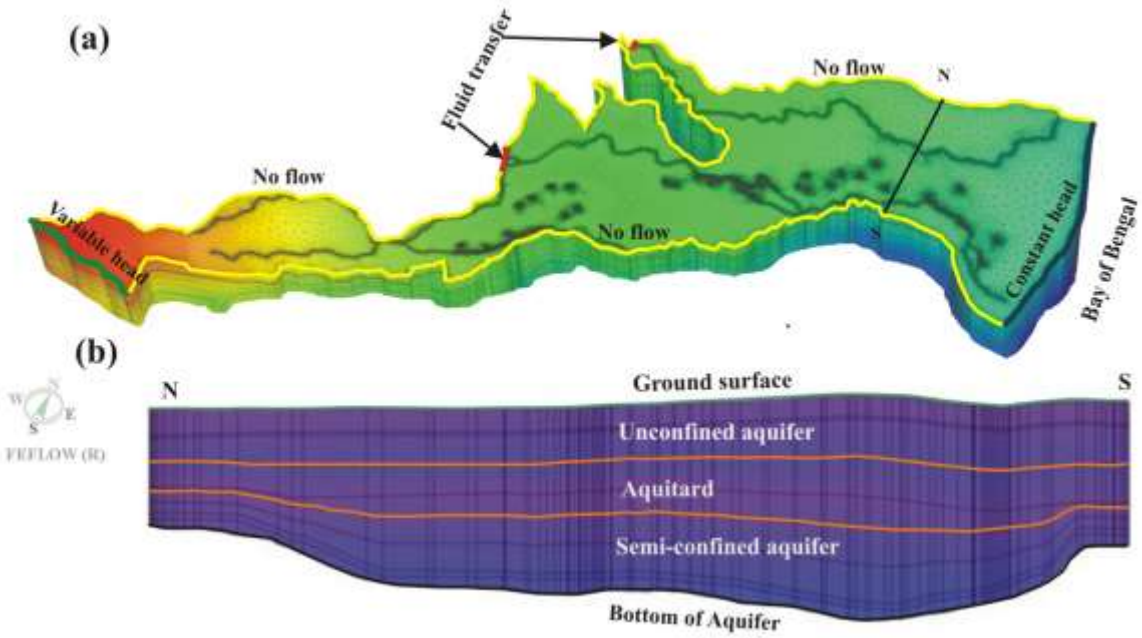

Fig. 3 (a) Perspective view of the three-dimensional discretization of the aquifer system **(b)** North south cross section

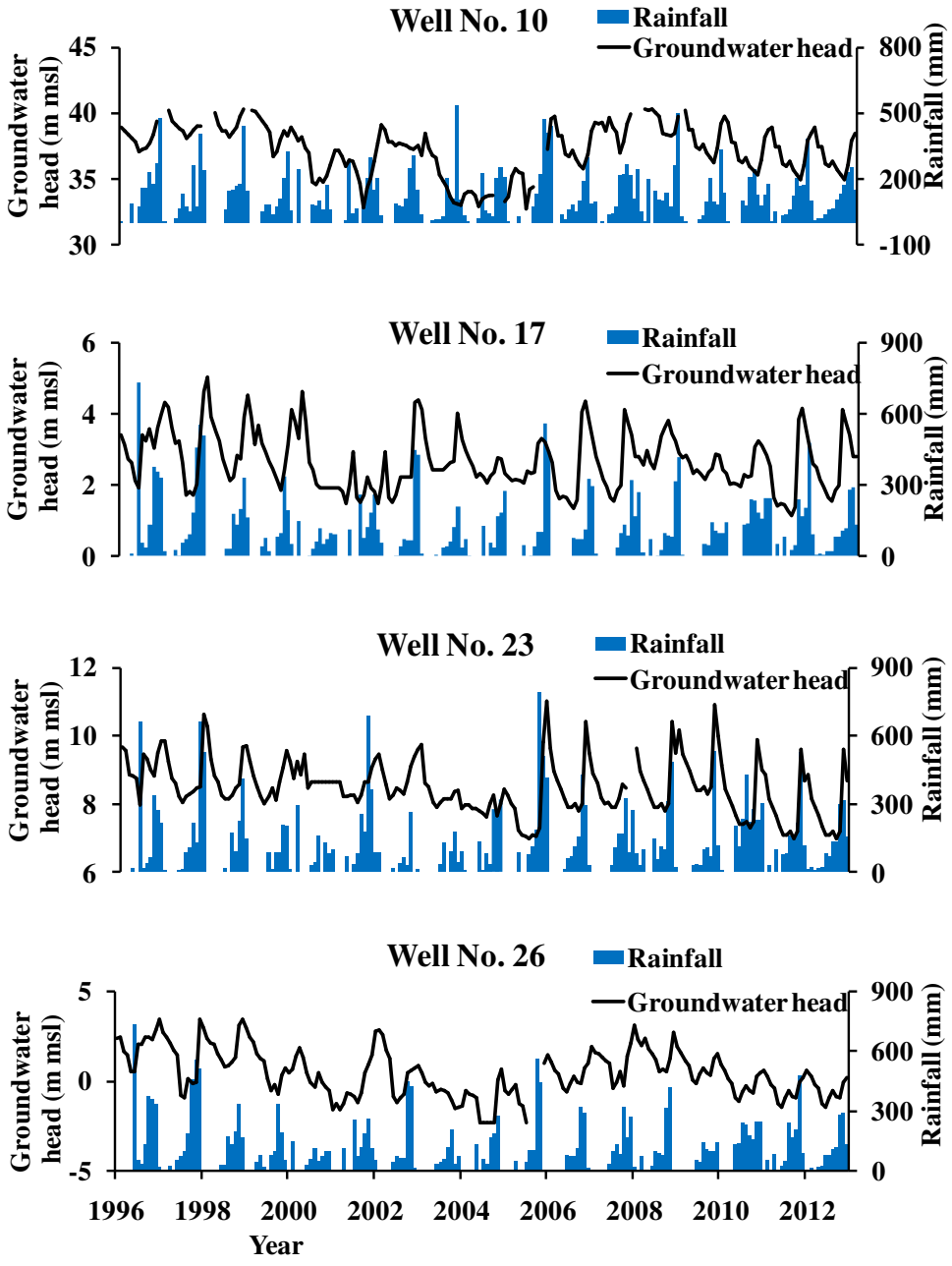

Fig. 4 Monthly variations in rainfall and groundwater head in the unconfined aquifer

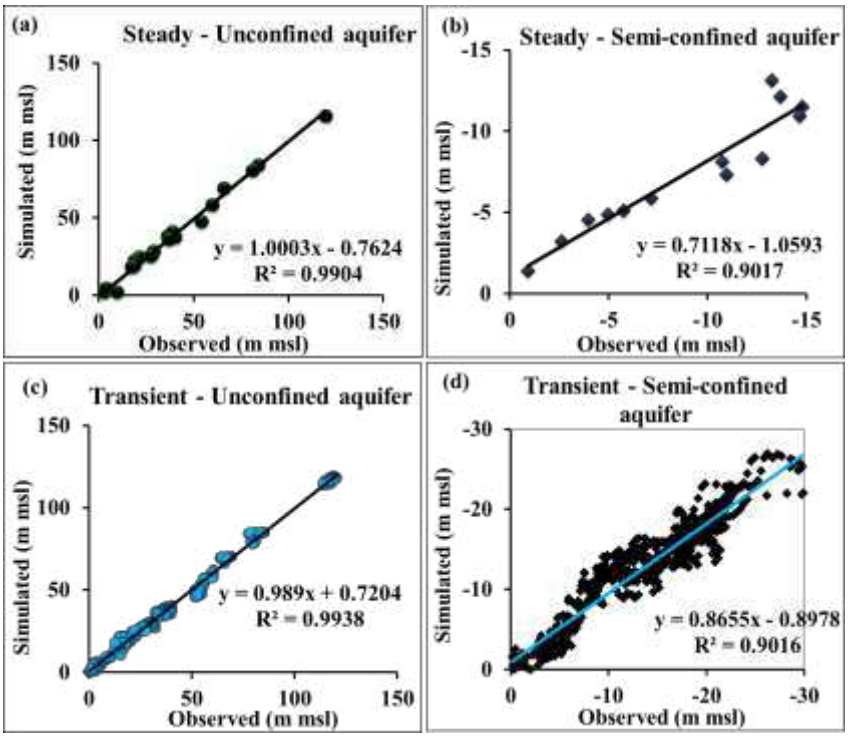

Fig. 5 Observed and simulated groundwater heads in steady state (**a**) unconfined aquifer (**b**) semi-confined aquifer, in transient state (**c**) unconfined aquifer (**d**) semi-confined aquifer

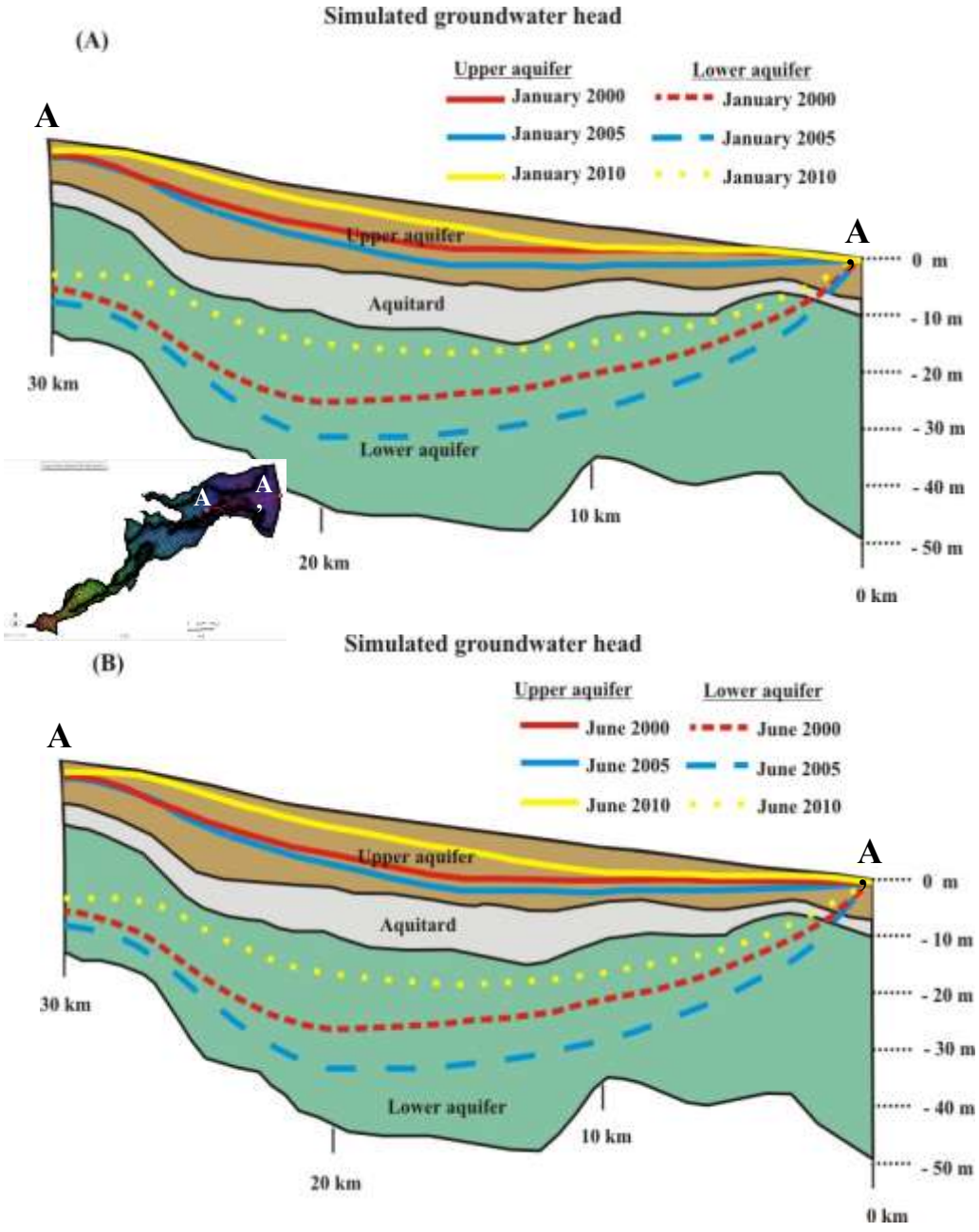

Fig. 6 Simulated groundwater head showing in the aquifer cross-section (a) January and (b) June for the years 2000, 2005 and 2010

872

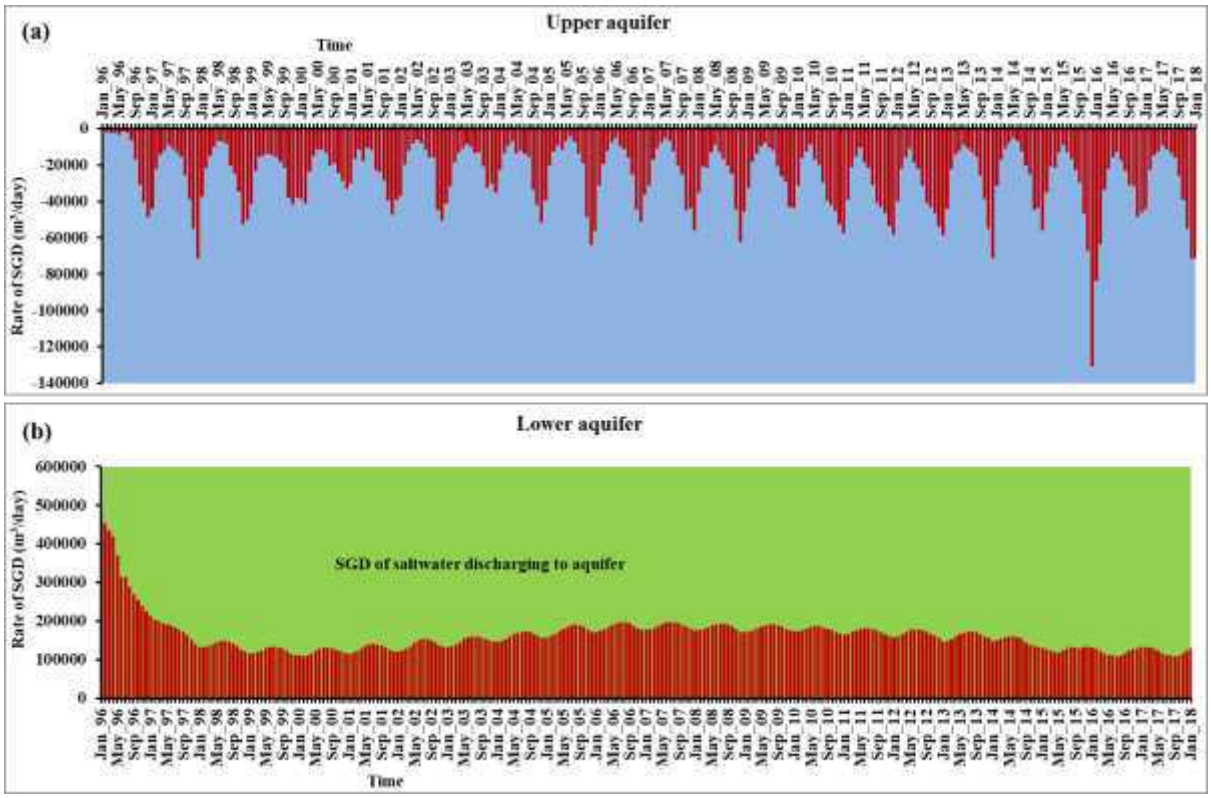

873

874

875 **Fig. 7** Temporal variations of total SGD along the eastern boundary **(a)** unconfined

876 aquifer **(b)** semi-confined aquifer

877

878

879

880

881

882

883

884

885

886

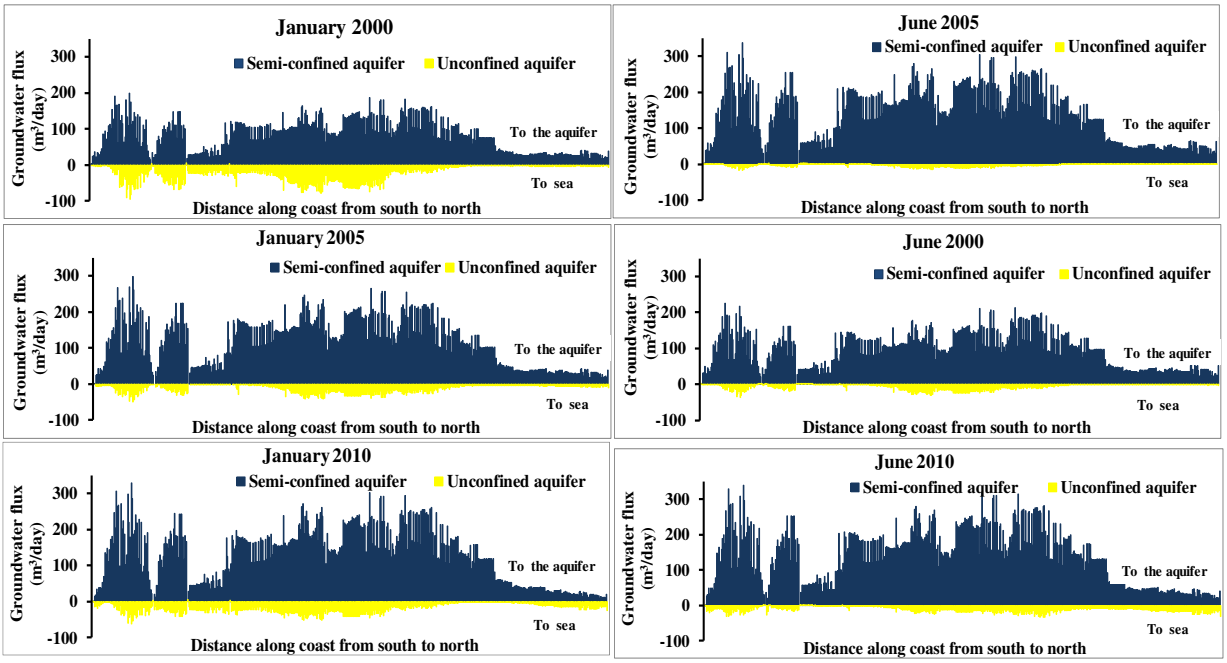

Fig. 8 Total groundwater flux along the eastern boundary **(a)** January 2000, 2005 and 2010 **(b)** June 2000, 2005 and 2010

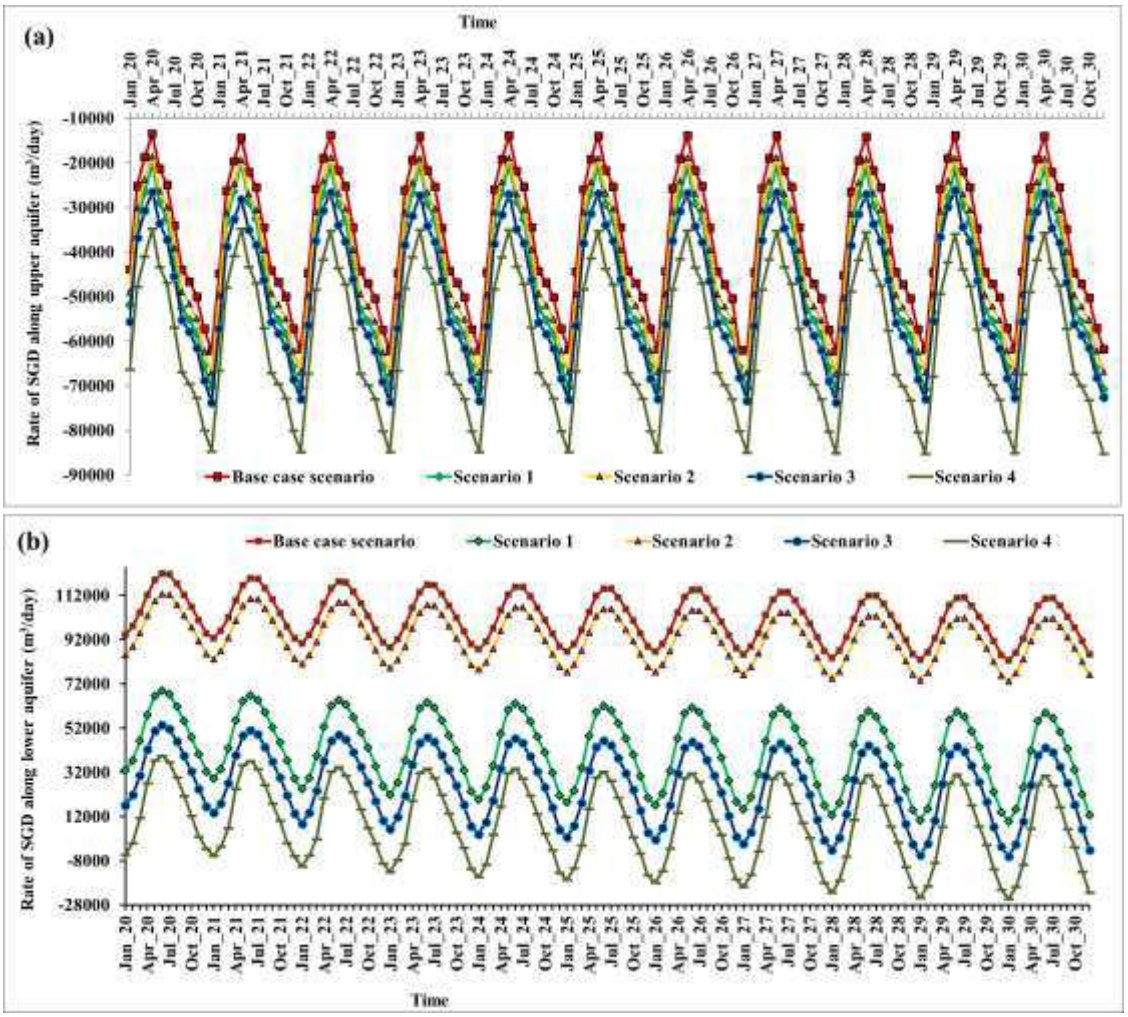

Fig. 9 Predicted rate of SGD along the eastern boundary in the **(a)** unconfined aquifer **(b)** semi-confined aquifer

Figures

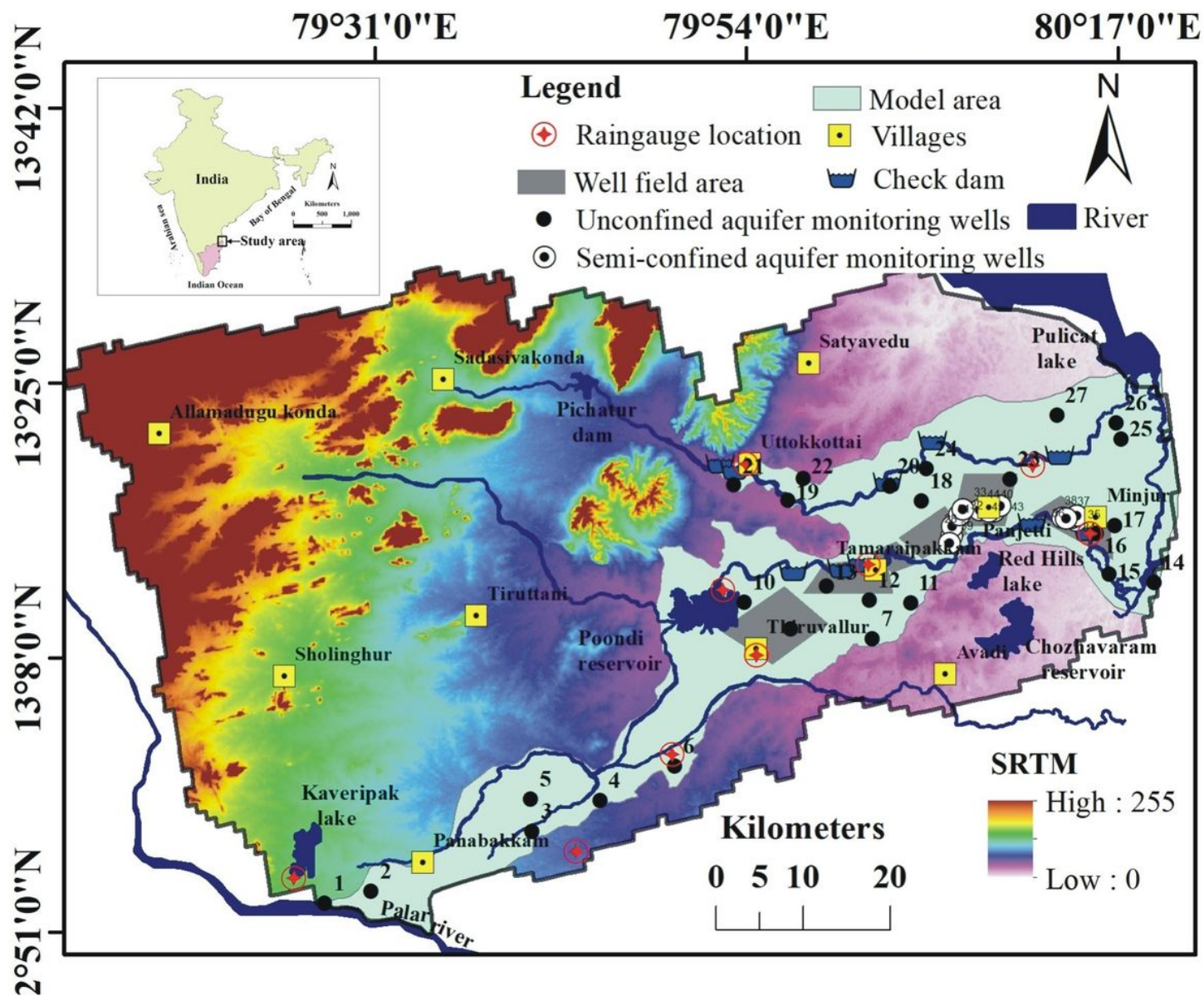

Figure 1

Location of the study area Note: The designations employed and the presentation of the material on this map do not imply the expression of any opinion whatsoever on the part of Research Square concerning the legal status of any country, territory, city or area or of its authorities, or concerning the delimitation of its frontiers or boundaries. This map has been provided by the authors.

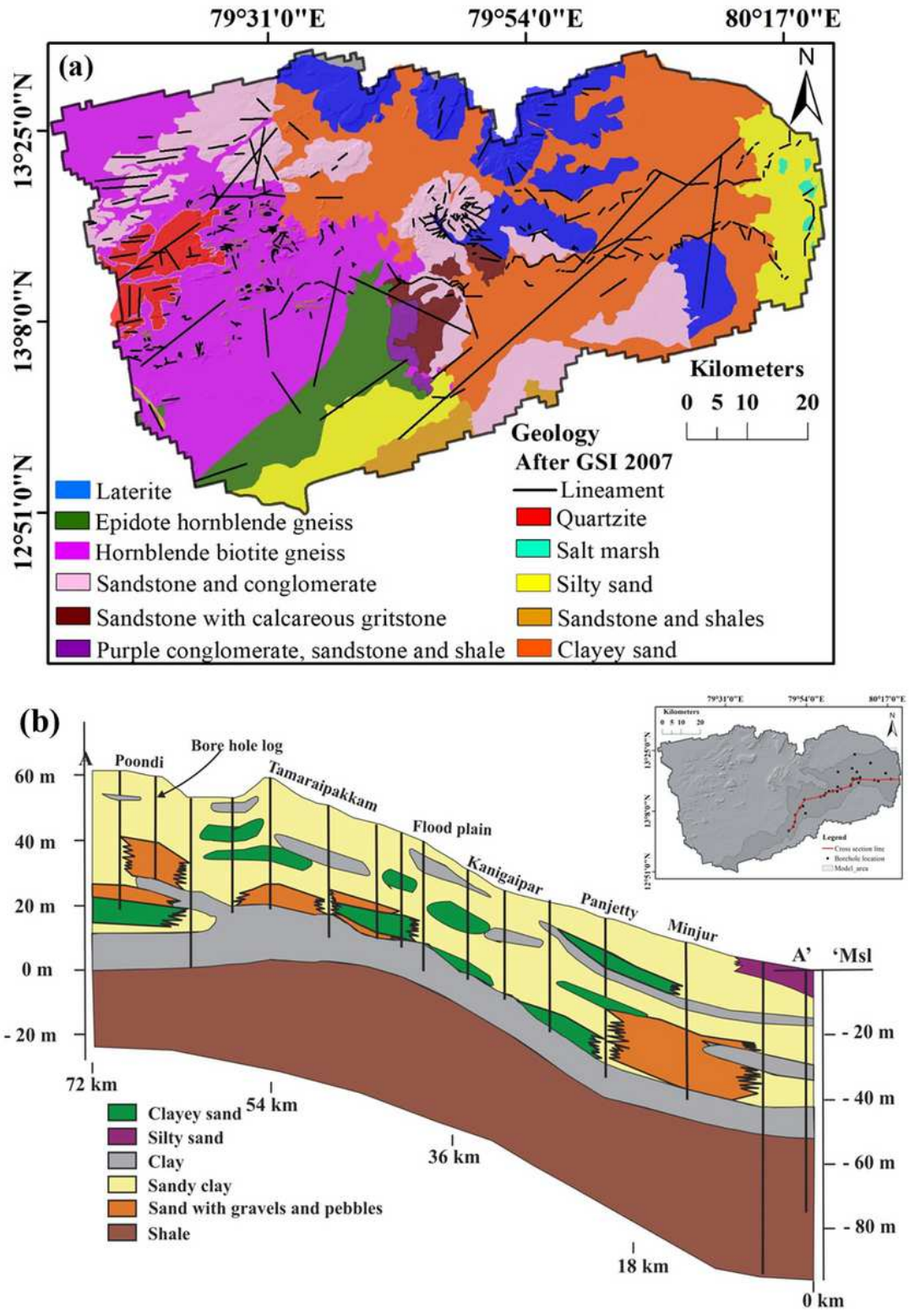

Figure 2

(a) Geology of the study area (b) West to east geological cross section along A-A' Note: The designations employed and the presentation of the material on this map do not imply the expression of any opinion whatsoever on the part of Research Square concerning the legal status of any country, territory, city or area or of its authorities, or concerning the delimitation of its frontiers or boundaries. This map has been provided by the authors.

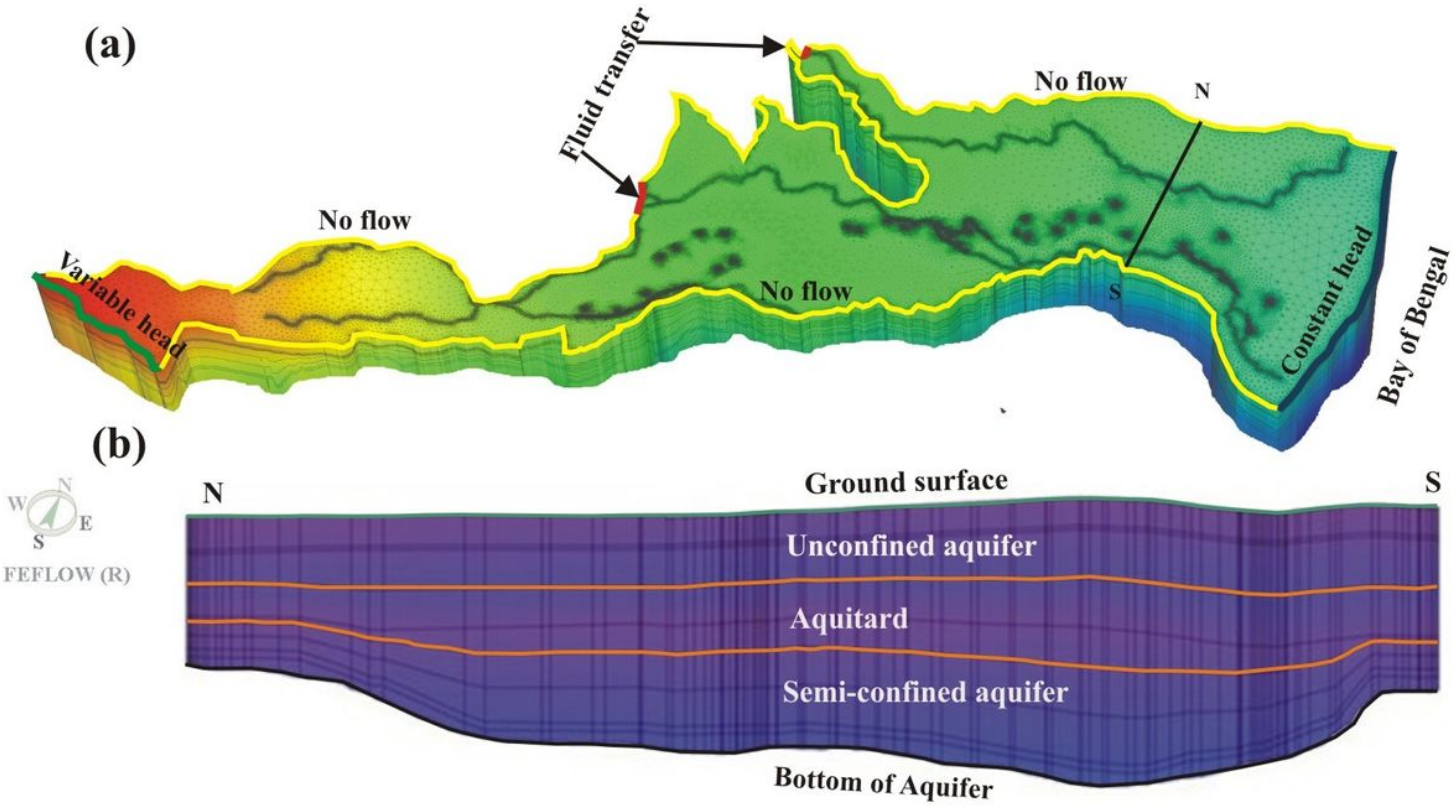

Figure 3

(a) Perspective view of the three-dimensional discretization of the aquifer system (b) North south cross section Note: The designations employed and the presentation of the material on this map do not imply the expression of any opinion whatsoever on the part of Research Square concerning the legal status of any country, territory, city or area or of its authorities, or concerning the delimitation of its frontiers or boundaries. This map has been provided by the authors.

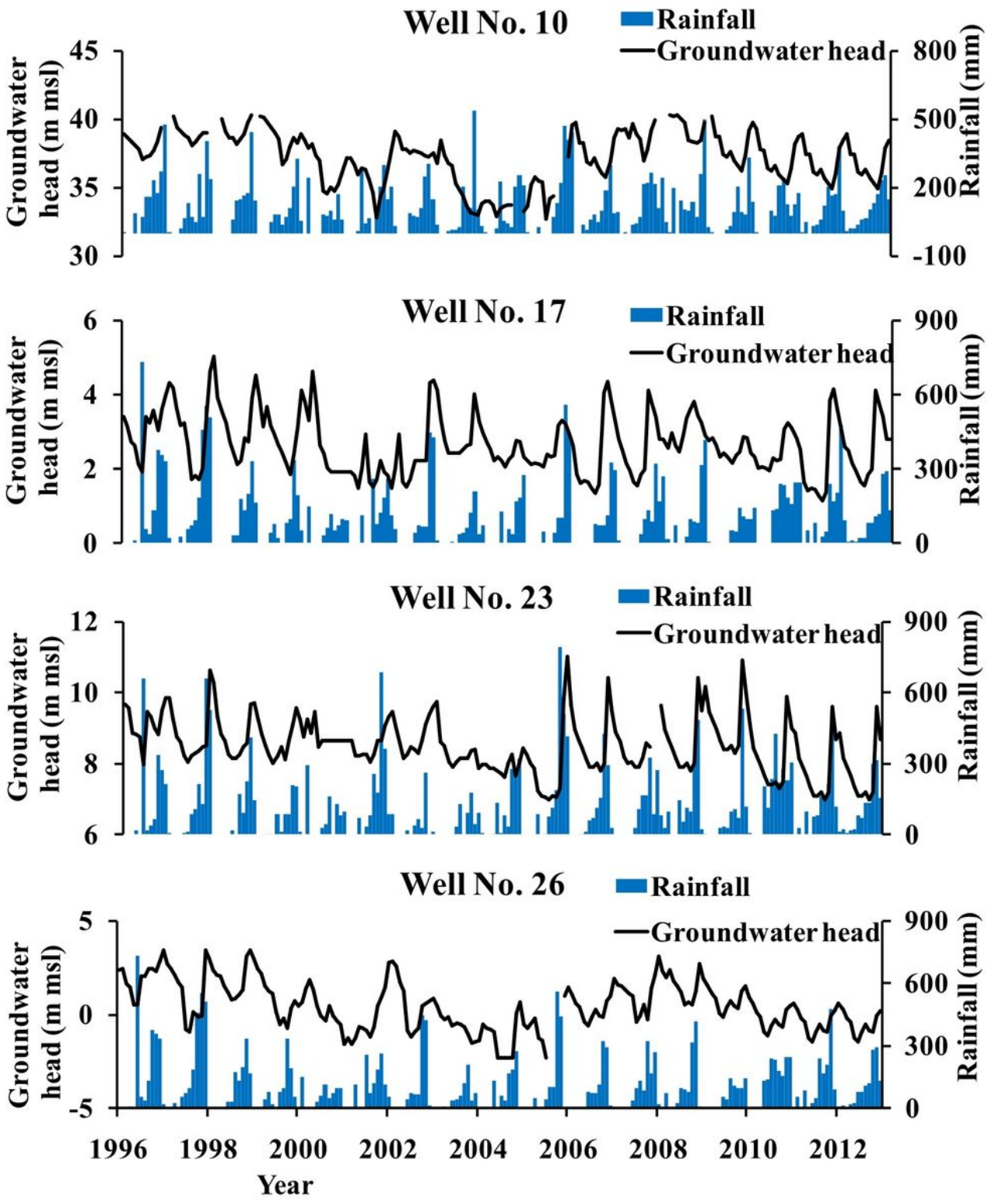

Figure 4

Monthly variations in rainfall and groundwater head in the unconfined aquifer

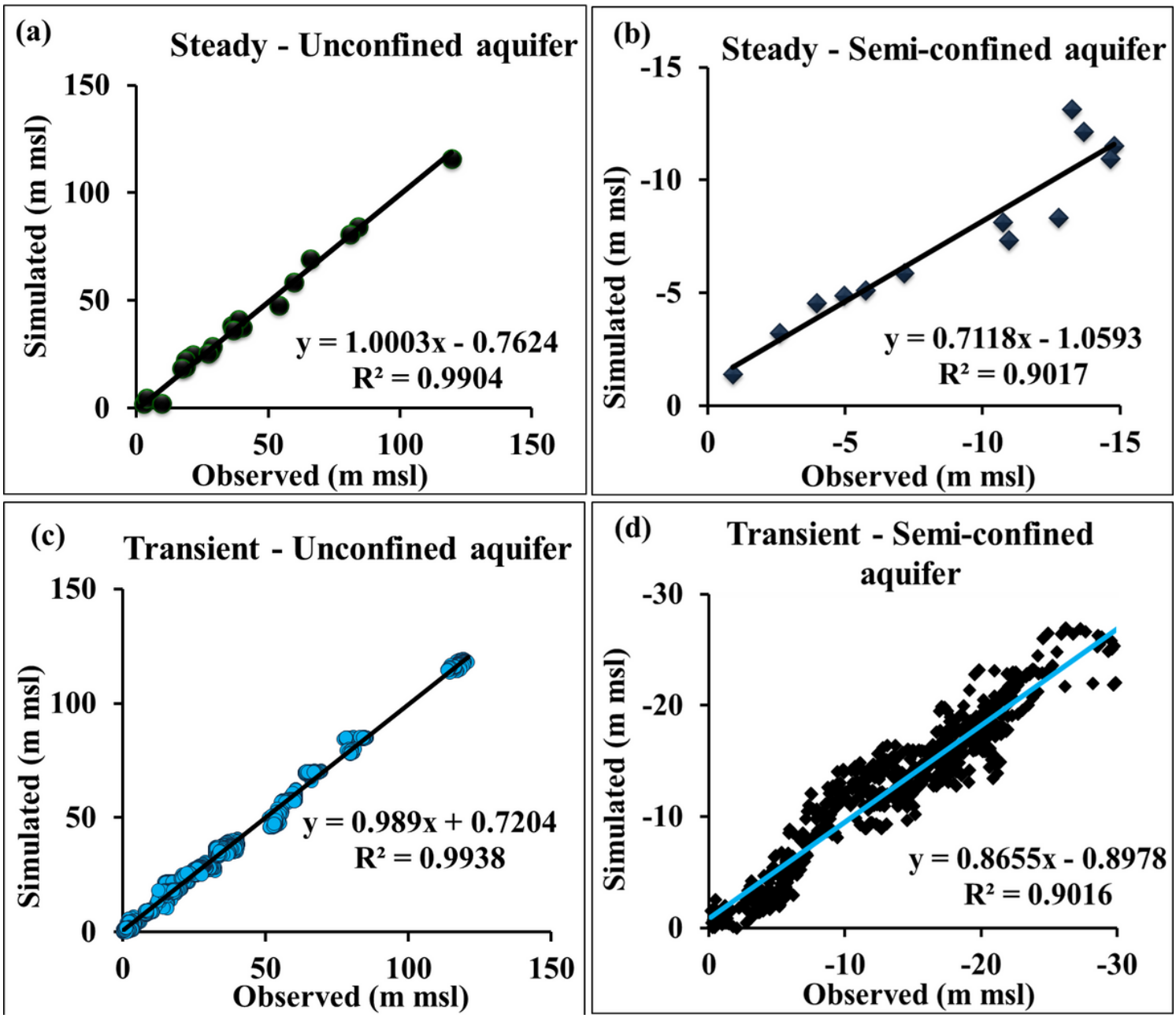

Figure 5

Observed and simulated groundwater heads in steady state (a) unconfined aquifer (b) semi-confined aquifer, in transient state (c) unconfined aquifer (d) semi-confined aquifer

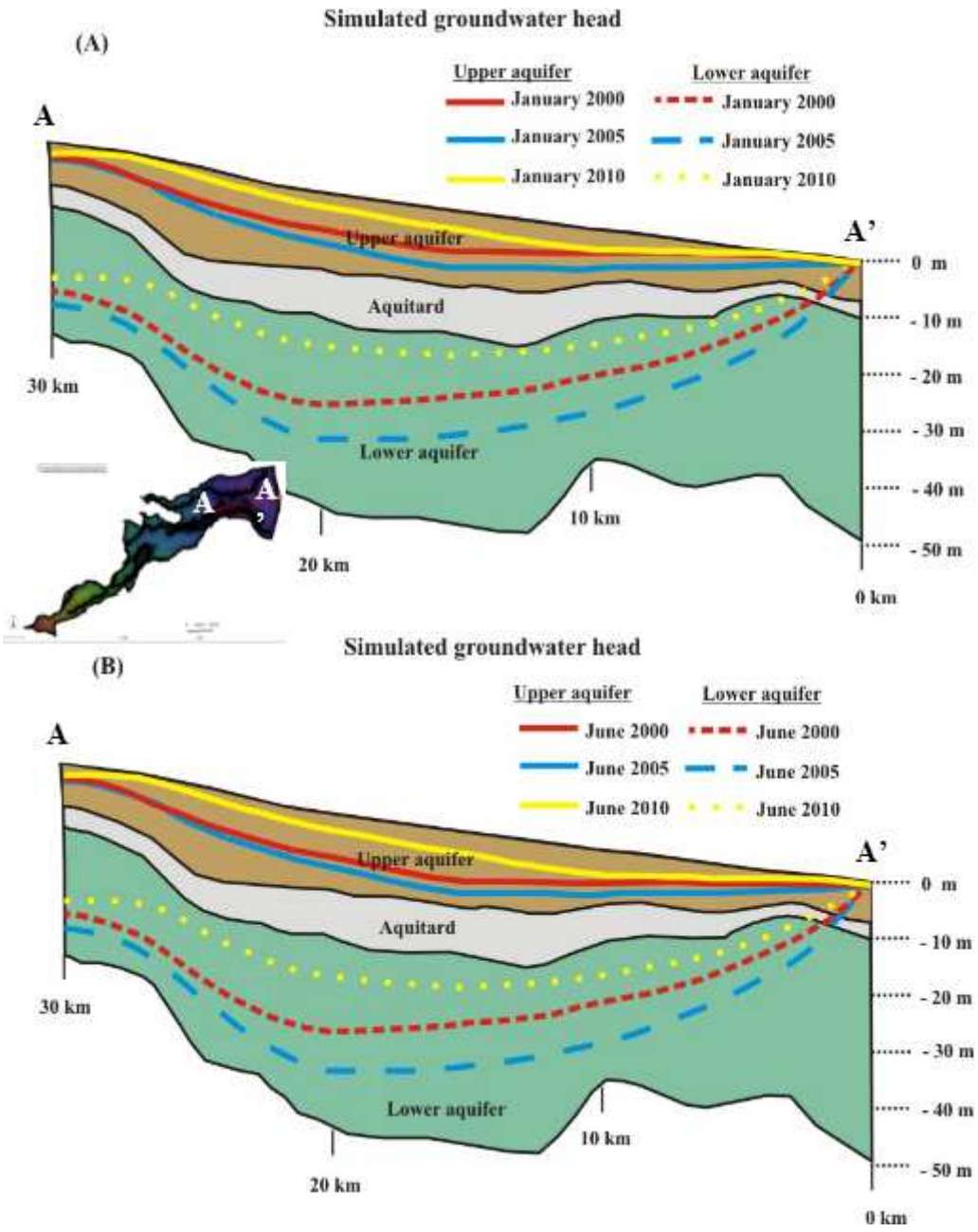

Figure 6

Simulated groundwater head showing in the aquifer cross-section (a) January and (b) June for the years 2000, 2005 and 2010 Note: The designations employed and the presentation of the material on this map do not imply the expression of any opinion whatsoever on the part of Research Square concerning the legal status of any country, territory, city or area or of its authorities, or concerning the delimitation of its frontiers or boundaries. This map has been provided by the authors.

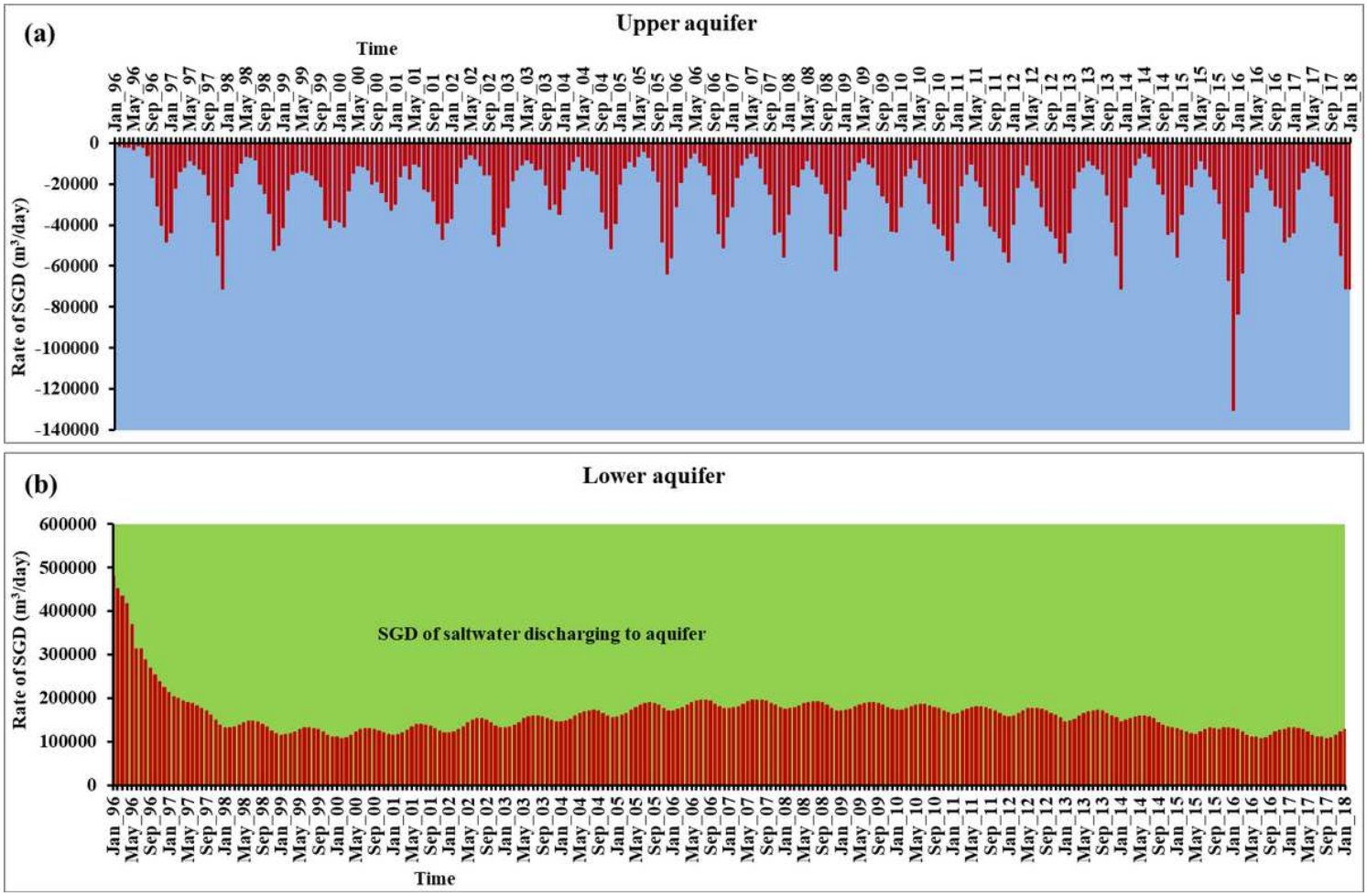

Figure 7

Temporal variations of total SGD along the eastern boundary (a) unconfined aquifer (b) semi-confined aquifer

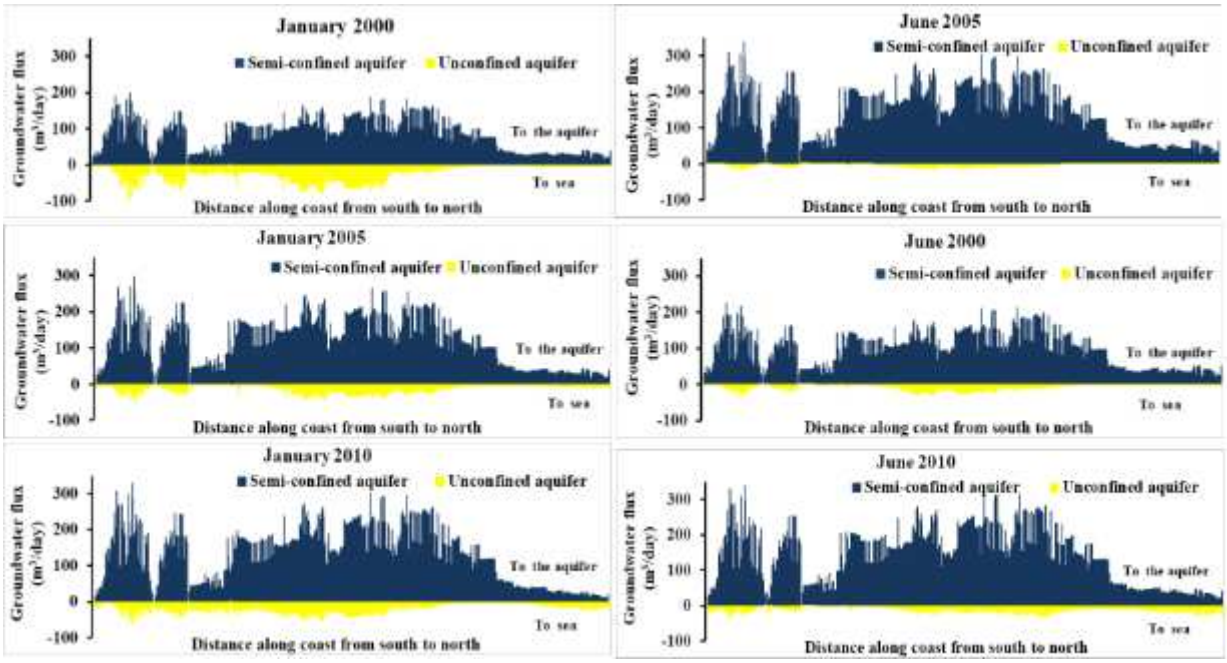

Figure 8

Total groundwater flux along the eastern boundary (a) January 2000, 2005 and 2010 (b) June 2000, 2005 and 2010

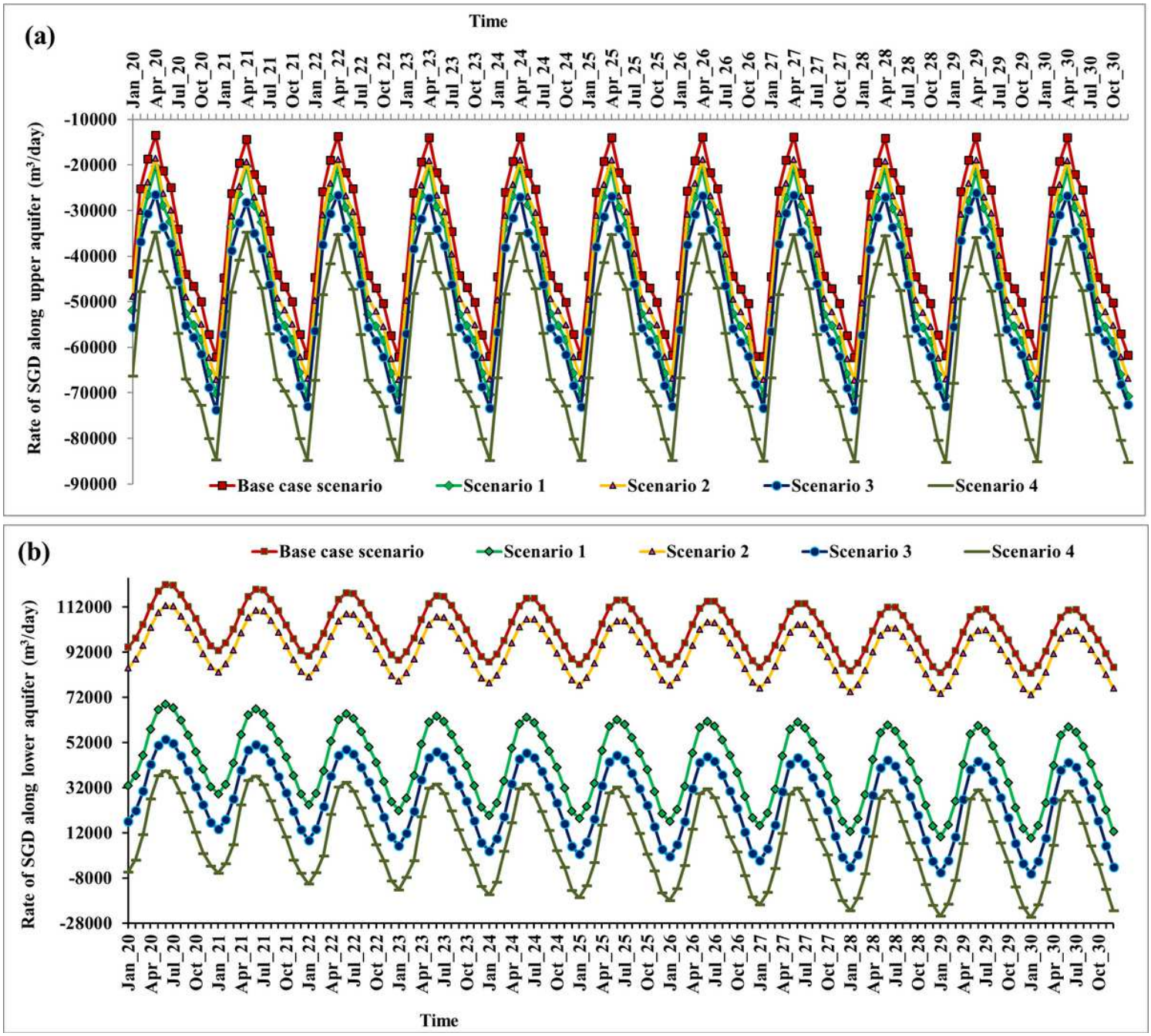

Figure 9

Predicted rate of SGD along the eastern boundary in the (a) unconfined aquifer (b) semi-confined aquifer